# Springback of a fully-clamped metallic beam loaded impulsively

**Jianwei Ren · Zhenyu Zhao · Yilai Zhou · Lusheng Qiang · Tian Jian Lu**

**Abstract** Upon impulsively loading a fully-clamped steel beam by firing a metallic foam projectile via a light-gas gun, a significant gap was experimentally observed between its transient peak deflection monitored during impacting and its permanent (residual) deflection measured after the impact was complete, i.e., springback had occurred. Finite element (FE) simulations were then performed to provide details concerning the evolution of stress and strain distributions as well as the initiation and traveling of plastic hinges in the beam, and the numerically calculated peak and residual deflections compared favorably with those measured experimentally. Subsequently, based upon the three distinct stages identified for the dynamically loaded beam, a beam-hinge analytical model was established to predict its springback response under sufficiently large uniform impulse, such that a portion of the beam or the entire beam was plastically yielded. The analytical predictions were compared with FE simulation results, with good agreement achieved. The validated model was then employed to systematically study the evolution of springback, the peak springback, the key factors affecting the magnitude of peak springback, and the roles played by different components constituting the internal energy stored in the beam. It was demonstrated that, as the impulsive load was increased, springback increased within the elasticity-dominated stage but decreased within the plasticity-dominated stage; the beam made of a metal having a higher yield strength exhibited a smaller peak deflection and a greater capacity to store elastic strain energy. Additional FE simulations revealed that strain hardening and strain rate effect led to further enhancement of springback. The present study clearly showed that springback is significant in dynamically loaded metallic structures, and hence should be accounted for in not only the design of practical protective structures but also their performance assessment.

**Keywords** Springback · Impulsive load · Fully-clamped metallic beam · Analytical model · Finite element simulation

J. Ren · Z. Zhao (✉) · Y. Zhou · L. Qiang · T. J. Lu (✉)
State Key Laboratory of Mechanics and Control of Mechanical Structures, Nanjing University of Aeronautics and Astronautics, Nanjing 210016, People's Republic of China
e-mail: sufengxing@foxmail.com

T. J. Lu
e-mail: tjlu@nuaa.edu.cn

J. Ren · Z. Zhao · Y. Zhou · L. Qiang · T. J. Lu
MIIT Key Laboratory of Multifunctional Lightweight Materials and Structures, Nanjing University of Aeronautics and Astronautics, Nanjing 210016, People's Republic of China

## 1 Introduction

In metal forming, removing a sample from a die often brings unloading of the forming forces, causing elastic shape change of the sample that has long been known as springback or rebounding (Marciniak et al. 2002; Hosford and Caddell 2007), as shown schematically in Fig. 1a. Similarly, the unloading of a transient impulse transmitted to a metallic structure can lead to springback of the structure (Karthikeyan et al. 2013; Russell et al. 2012; Olovsson et al. 2010). Particularly, in extreme loading circumstances such as high velocity impacting and explosive blast loading, significant structural springback has been observed via experimental measurements and numerical simulations (Qiu et al. 2005; Liu et al. 2013; Hawass et al. 2005). For example, as shown in Fig. 1b, double-floor design has

been widely adopted in armored vehicles to protect against shallow-buried mines (Showichen 2008). Upon detonation, the bottom plate achieves firstly a transient peak deflection, causing collision with the top plate if the impulse is sufficiently intense such that the latter also starts to deflect upward. Towards the end of the impulsive loading, both the top and bottom plates would most likely rebound and hence their deflections decrease from the peaks, affecting both occupants and equipment in the vehicle. Figure 3a depicted experimentally the temporal evolution of deflection of a fully-clamped plate subjected to transient impulsive loading. Upon loading, the deflection of the plate increases sharply, reaches a peak $\delta_m$ before decreasing, and then fluctuates with gradual reduction in fluctuation magnitude until reaching a stable residual (permanent) deflection $\delta_r$ due to



(a)



(b)
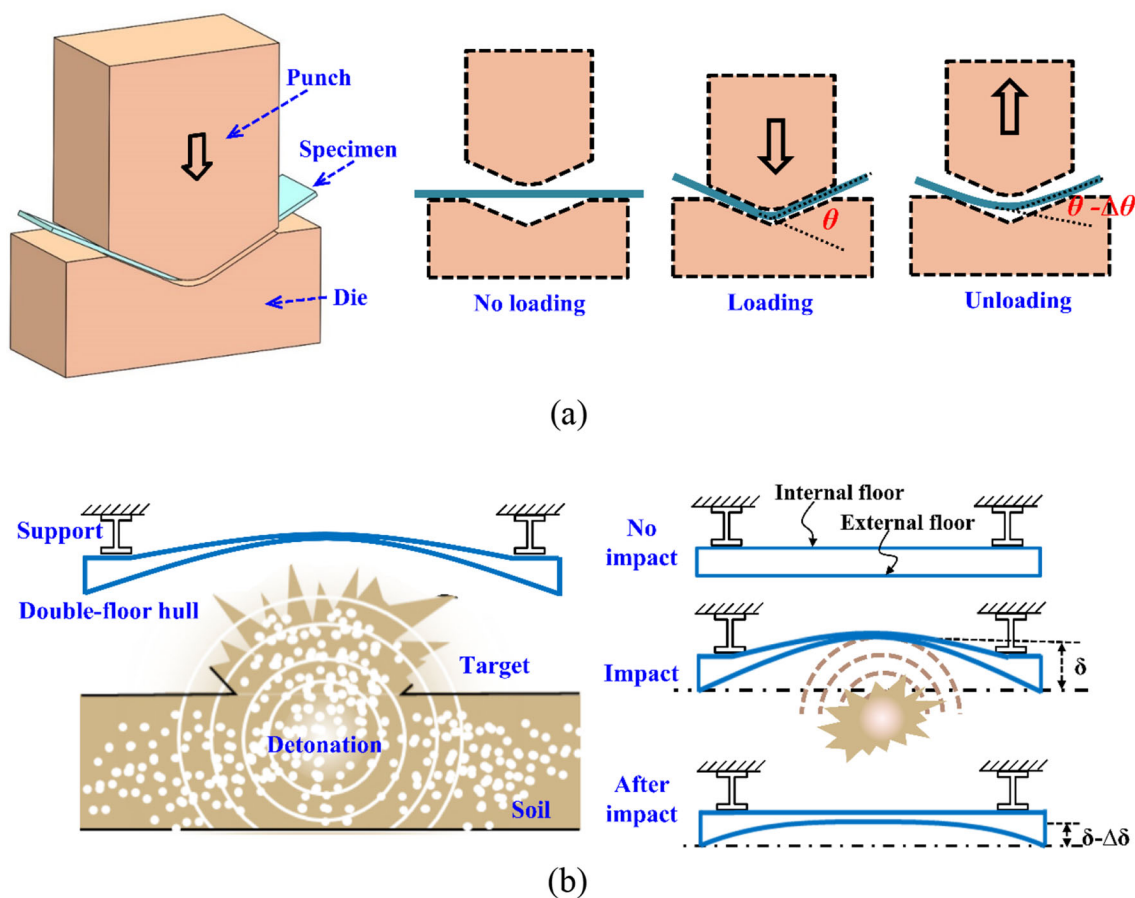
**Fig. 1** Schematic of **a** quasi-static springback in metal forming and **b** springback in a double-plate metallic structure subjected to blast loading

structural damping. The gap between $\delta_m$ and $\delta_r$ has often been defined as springback (Schleyer et al. 2003; Remennikov and Uy 2014; Wu et al. 2020), an important feature that should not be overlooked in any dynamic structural design.

When subjected to intense impact loading, the response process of a structure typically develops within an extremely short time period. Further, during the explosion of shallow-buried charges (mines), the explosion fire and detonation products often obscure (temporarily) the deflection profile of the loaded structure, such that measuring its peak deflection with high-speed photography is extremely difficult (Kyner et al. 2017a, 2017b). Consequently, at present, the design of a protective structure against blast loading relies predominantly on its residual (permanent) deflection measured after the loading is complete, rather than its peak (maximum) deflection achieved during the transient process of its deformation (Wu et al. 2020; Schleyer and Hsu 2000; Radford et al. 2005; Rathbun et al. 2006). However, although it is known that transient peak deflection occurs in many metallic structures loaded impulsively (Karthikeyan et al. 2013; Russell et al. 2012; Olovsson et al. 2010; Liu et al. 2013; Xue and Hutchinson 2004), how it affects the protective performance of the structure remains elusive. It is therefore necessary to assess the protective performance of the design from not only the residual deflection of the structure, but also its (transient) peak deflection and springback achieved during dynamic deformation.

The springback of a metallic structure, either quasi-static or dynamic, is strongly dependent upon the properties of its material make (Marciniak et al. 2002; Zhang et al. 2007; Da-Xin et al. 2009). With particular focus placed upon quasi-static scenarios, existing studies have mainly been carried out to explore the variation trend and influential factors of springback. For example, during forming, when a metallic sheet exhibits a sufficiently small permanent deflection, its springback is found to be dominated by the yielding strength and elastic modulus of its parent material (Marciniak et al. 2002; Zhang et al. 2007). Similarly, significant springback of a bent metallic tube occurs upon removing loading during pure elastic deformation, whereas plastic deformation has little contribution to springback of the bent tube (Da-Xin et al. 2009). In contrast, when subjected to dynamic loading, the springback of a metallic structure has mainly been

identified on the basis of its temporal deflection changing curves, either experimentally or theoretically (Karthikeyan et al. 2013; Russell et al. 2012; Olovsson et al. 2010; Hawass et al. 2005; Remennikov and Uy 2014; Neuberger et al. 2007). At present, few studies have focused specifically upon the phenomenon of structural springback under dynamic loading and its underlying physical mechanisms. Experiments with pressure pulse on a clamped metallic plate revealed that its springback varies as the plate size or magnitude of pressure is varied (Schleyer et al. 2003). When subjected to air-blast loading, the springback of a metallic plate first tends to increase and then decrease as its residual (permanent) deflection is increased (Neuberger et al. 2007, 2009). For a dynamically loaded plate, although an earlier study indicated that the variation of springback is relevant to competing elastic and plastic deformations in the plate (Neuberger et al. 2009), further clarification of its mechanisms is a necessity.

This study aimed to investigate the springback of a fully-clamped metallic beam loaded impulsively, with focus placed upon the evolution of springback, the peak springback, the key factors affecting the magnitude of peak springback, and the roles played by different components constituting the internal energy stored in the beam. The paper is organized as follows. In Sect. 2, by simulating the blast loading by firing a metallic foam projectile via a light-gas gun, impact test was performed on a fully-clamped beam made of high-strength armor steel to provide preliminary experimental evidence of structural springback. In addition to impact testing, in Sect. 3, the method of finite elements (FE) was employed to simulate the springback phenomenon and explore in detail its underlying physical mechanisms. In Sect. 4, based upon the three distinct stages of springback identified for the impulsively loaded, fully-clamped metallic beam, an analytical beam-hinge model of springback was developed: particular focus was placed upon sufficiently large impulses such that a portion of the beam or the entire beam is plastically yielded. In Sect. 5, analytical predictions were compared with FE simulation results for fully-clamped beams made of various alloys (steel, aluminum and titanium), and the effects of yield strength, strain hardening and strain rate on springback were quantified. Section 6 was devoted to revealing the importance of accounting for

the effect of springback in the practical design of protective structures against blast loading.

## 2 Springback experiment

### 2.1 Experimental procedures

It has been demonstrated that an impulsive load could be simulated via the impacting of a metallic foam metal projectile fired via a light-gas gun (Radford et al. 2005; Russell et al. 2012; Li et al. 2019). The same technique was employed by the present study so that the springback performance of a fully-clamped metallic beam could be captured experimentally.

Figure 2a presented the impact test system, including all employed apparatuses and boundary condition of the test specimen. Impulsive loading at the central region of the specimen was achieved by firing a cylindrical projectile (diameter $d_p = 58$ mm and

length $h_p = 100$ mm) from a light-gas gun. The projectile was made of a closed-cell aluminum foam available commercially, with a density of $\rho_p$ 378 kg/m³ and a plateau compressive stress of 3.2 MPa. A laser gauge was used to measure the impacting velocity of the projectile, as sketched in Fig. 2a, while a high-speed photographic system, including a high-speed camera (IX-SPEED 716) and two high intense illuminators, was placed on the side of the light-gas gun to capture the structural response of the dynamically loaded beam. With the frame rate fixed at 20,000 fps, the camara was triggered at the moment when the foam projectile was launched. In the present preliminary test, the foam projectile had a fixed mass of 100 g and a fixed impact velocity of $\sim$ 240 m/s.

The tested beam (length 370 mm, width 60 mm, and thickness 6 mm; Fig. 2b) was made of a specific type of armor steel manufactured and supplied by Nanjing Iron & Steel United Co., Ltd., China), with density 7800 kg/m³, Young's modulus 210 GPa, and
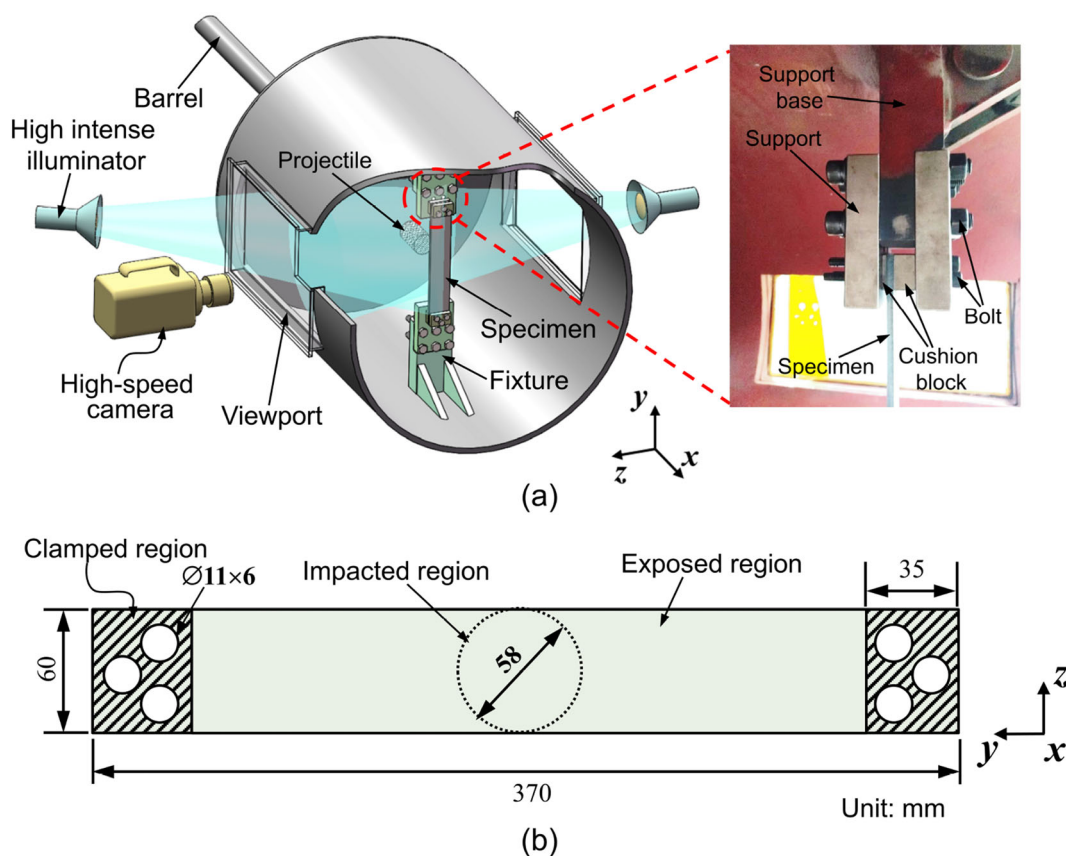


Fig. 2 a Schematic of light-gas gun setup for impact testing of clamped beam, and b geometry of test specimen

static yield strength 1072 MPa. At each end of the beam, there were three staggered bolt holes so that it could be clamped with the support via M12.9 bolts (10 mm in diameter). Based on an existing support base (made of Q235 steel) that was welded onto the barrel of the light-gas gun (as shown in Fig. 2a), a fixing strategy was purposely designed so that fully-clamping of the beam could be realized. Due to the significantly higher yield strength (1027 MPa; Table 1) of the beam material make than that (270 MPa; Table 1) of the support base, additional clamping support plate (20 mm thick) was mounted onto each side of the L-shaped support base to limit the displacement of the beam at its distal ends. Because the beam tested was much thinner than that of the support base plate, a gap was present between the two; as a result, cushion blocks were used to fill the gap, as shown in Fig. 2a. Both the clamping supports and the cushion blocks were made of 45# steel (yield strength 210 MPa). The beam and its support plates were fixed onto the base plate by means of six high-strength bolts (16 mm diameter), as shown in Fig. 2a, to ensure a clamped boundary condition.

## 2.2 Experimental measurements

Figure 3a plotted the measured mid-point deflection of the fully-clamped armor steel beam as a function of time, while Fig. 3b displayed selected images showing its temporal deformation, corresponding to the points marked on Fig. 3a. It was seen that significant springback occurred in the impulsively loaded steel beam. From Fig. 3a, after multiple cycles of rebounding, the beam reached its permanent deflection when it became motionless, which was significantly less than

its peak deflection (achieved at point 3 in Fig. 3a). Correspondingly, as shown in Fig. 3b, upon reaching the peak deflection at 0.95 ms, the beam started to rebound towards its original position, indicating that springback occurred. Additionally, it was seen that the aluminum foam projectile braced against the impacted zone of the beam, during which its front was gradually crushed, generating ejected foam debris.

It should be pointed out that, although the impact test performed was only preliminary because the focus of the present study was placed upon analytical modeling, the test served two main purposes: (a) provide clear experimental evidence of springback in an impulsively loaded metallic beam, and (b) enable direct comparison between experimental measurements of springback with numerical simulations detailed in the next section so that the simulations could be validated. Subsequently, as the present experimental setup could not provide uniform impulsive loading on a fully-clamped beam considered by the proposed analytical model, the model predictions were validated using numerical simulation results. In a separate study, built upon the present results of analytical modeling and numerical simulation, a series of dynamic tests will be conducted to systematically characterize the springback behaviors of different metallic structures.

## 3 Numerical simulation

### 3.1 Validation of finite element modeling

In addition to impact testing detailed in the previous section and analytical modeling to be presented in

**Table 1** Material parameters of armor steel, 45# steel and Q235 steel

| Type of steel | | Armor steel | 45 # steel | Q235 steel |
|---|---|---|---|---|
| Density | $\rho$ (kg/m$^3$) | 7800 | 7800 | 7850 |
| Elastic Modulus | $E$ (GPa) | 210 | 210 | 206 |
| Yield Strength | $\sigma_y$ (MPa) | 1027 | 507 | 270 |
| Poisson ratio | $v$ | 0.3 | 0.3 | 0.3 |
| Strain hardening constant | $B$ (MPa) | 1030 | 320 | 275 |
| Strain hardening exponent | $n$ | 0.77 | 0.28 | 0.36 |
| Strain rate hardening | $C$ | 0.01 | 0.064 | 0.022 |
| Reference strain rate | $\dot{\varepsilon}_0$ | 0.0001 | 1 | 1 |
| Reference | – | – | Chen et al. (2005) | Zheng et al. (2016) |
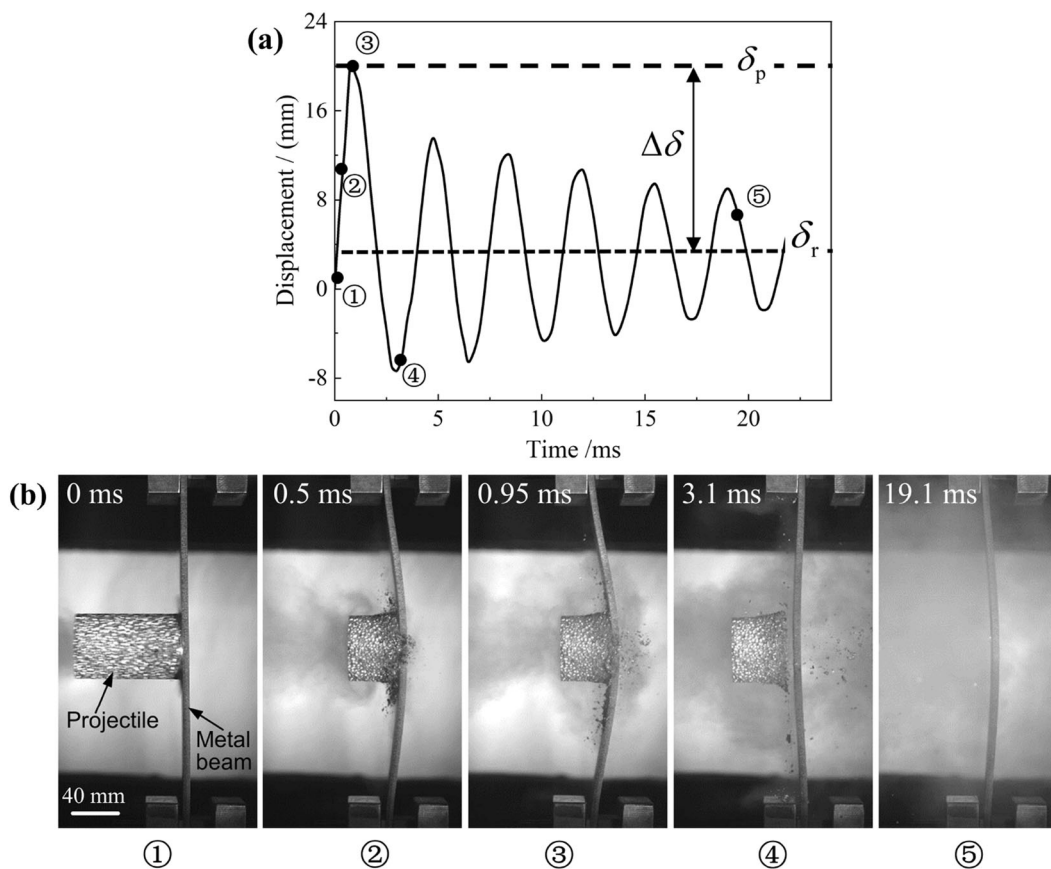
**Fig. 3** **a** Measured mid-point deflection of a fully-clamped steel beam (loaded impulsively by an aluminum foam projectile fired from a light-gas gun) plotted as a function of impact time, and **b** high-speed photography images showing springback of the beam

Sect. 4, numerical simulations of springback were also carried out using the method of finite elements (FE), based upon the following main assumptions:

(i) Upon impulsive loading, the kinetical energy of the fully-clamped beam is completely dissipated via structural deformation such that its total deformation energy is equal to its kinetical energy.

(ii) Throughout the dynamic loading process, no fracture occurs in the beam.

First, to validate the present FE simulation (conducted with ABAQUS), the impact case studied numerically by Xue and Hutchinson (2004) was revisited. To this end, the simulated metallic beam had a fixed configuration size of 1 m × 0.1 m × 0.02 m between two confining blocks (each 0.16 m in length; Fig. 4). Due to the extreme shortness of the

loading period, the uniform areal impulsive load duplicating typical blast loading was substituted by an initial imposed velocity on the loaded surface of the beam (Jones 2012). The applied initial velocity was determined by $V = I_0/\overline{M}$, where $I_0$ is the nominal impulse per unit area and $\overline{M}$ is the areal mass of the beam. The areal mass can be calculated as the product of mass density $\rho$ and beam thickness $H$, i.e., $\overline{M} = H\rho$. In accordance with Xue and Hutchinson (2004), the material make of the beam was selected as 304 SS stainless steel, with mass density $\rho = 8000$ kg/m$^3$, yielding strength $\sigma_y = 205$ MPa, elastic modules $E = 210$ GPa, plastic strain hardening parameter $N = 0.17$, and Poisson ratio $v = 0.3$.

With hexahedron meshing employed (Fig. 4), a meshing insensitivity was carried out. The normalized maximum beam deflection $\delta_m/L$ was plotted in Fig. 5a as a function of element size for the fully-
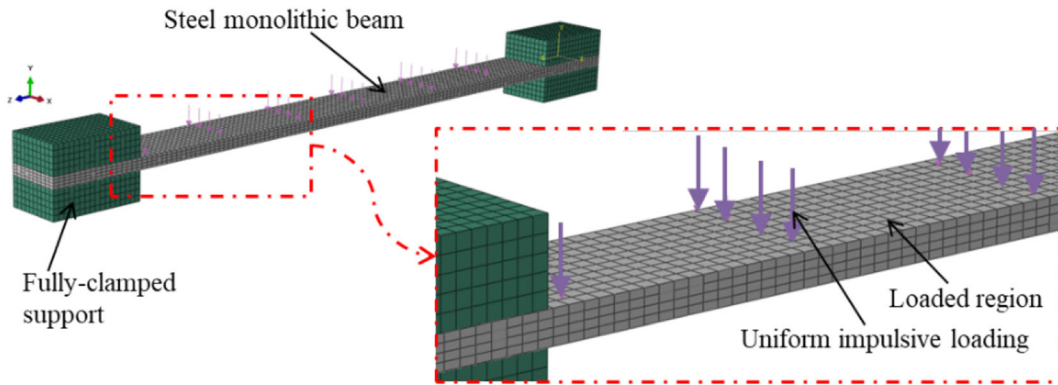
**Fig. 4** Finite element model of a fully-clamped metallic beam subjected to impulsive loading
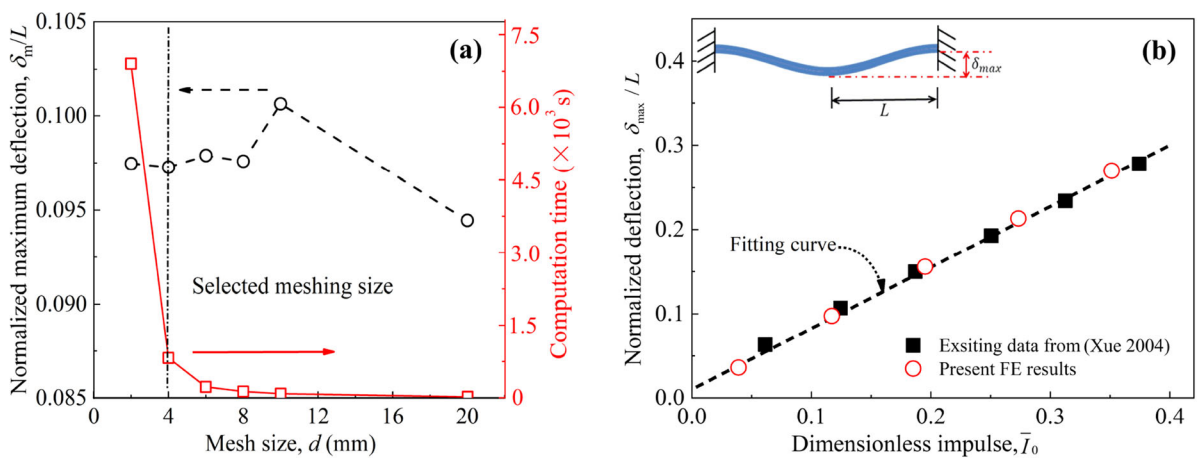


**Fig. 5 a** Mesh sensitivity study and **b** comparison between the present FE simulation results and those reported in a previous study (Xue and Hutchinson [2004]) for a fully-clamped 304 SS beam loaded by $\bar{I}_0 = 0.096$

clamped 304 SS beam loaded by a dimensionless impulse of $\bar{I}_0 = 0.096$. Here, $\bar{I}_0 = I_0/(\overline{M}\sqrt{\sigma_y/\rho})$ is a dimensionless coefficient quantifying the magnitude of the impulsive load. Correspondingly, the increase in the number of total elements with decreasing element size was also displayed in Fig. 5a. For balanced simulation accuracy and computational cost, the mesh size was selected as 4 mm for this case (as well as all subsequent numerical models).

For validation, in Fig. 5b, the numerical simulated $\delta_m/L$ versus $\bar{I}_0$ relation was compared with that calculated by Xue and Hutchinson (2004). It was seen that, over the entire range of $\bar{I}_0$ considered (from 0.04 to 0.38), excellent agreement was achieved. It should be pointed out that, as the structural deflection and springback of a dynamically loaded beam are strongly dependent upon its kinetic energy, the initial kinetic

energy $E_k$ was employed as the key loading variable in lieu of $\bar{I}_0$, with $E_k$ calculated from $\bar{I}_0$ via $\bar{I}_0 = \sqrt{2E_k/HBL\sigma_y}$.

### 3.2 Numerical simulation of impact test

Next, to compliment the experimentally observed springback phenomenon detailed in Sect. 2.1 and explore its underlying physical mechanisms, the impact test was simulated using the validated FE modeling. With reference to Fig. 6, a FE model was constructed, with all geometries of its components, including the loaded beam and the auxiliary parts, identical to those employed in the impact test. The support base was fixed by limiting its displacement and rotation in all directions. Same as the real impact test, two support plates were mounted onto the base

**Fig. 6** Finite element model of impact test with light-gas gun
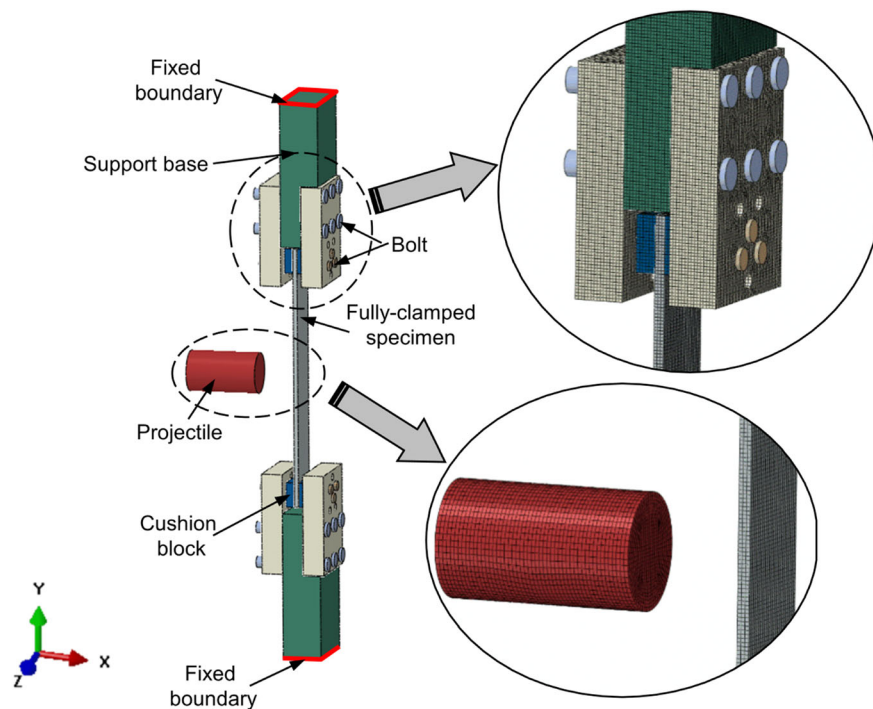
via six bolts, with each bolt set as rigid. The steel beam was fixed (also via bolts) between the two support blocks, and the gap was filled by cushion blocks. Contacts between all adjacent surfaces were set as "general contact" in ABAQUS, with no-friction achieved via a penalty algorithm. As mentioned in Sect. 2.1, the beam was made of armor steel, the cushion blocks and support plates were made of 45# steel, and the support base was made of Q235 steel. The material model for these steels was treated as the Johnson–Cook plasticity model, given by:

$$\sigma_{ys} = \left[\sigma_0 + B(\overline{\varepsilon}_{pl})^n\right]\left[1 + C\ln\left(\frac{\dot{\overline{\varepsilon}}_{pl}}{\dot{\varepsilon}_0}\right)\right] \qquad (1)$$

where $\sigma_{ys}$ is the rate-dependent yield stress, $\overline{\varepsilon}_{pl}$ is the equivalent plastic strain, $B$ and $n$ are the plastic hardening parameters, $C$ is the strain-rate constant, $\dot{\varepsilon}_0$ and $\dot{\overline{\varepsilon}}_{pl}$ are separately the reference strain rate and the equivalent plastic strain rate. The coefficients appearing in Eq. (1) were listed in Table 1 for each type of steel considered.

The numerically calculated mid-span deflection of the loaded beam was plotted as a function of time in Fig. 7. Similar to the measured deflection versus time curve of Fig. 3a, the simulated deflection first reached

a peak ($\delta_p$), followed by a sharp drop and then multiple cycles of rebounding, and eventually converged to a stable value—the residual deflection ($\delta_r$). From Fig. 7 it was seen that both the numerically predicted peak deflection $\delta_p$ and residual deflection $\delta_r$ were close to those measured experimentally, thus validating again the feasibility of the present FE simulation. Nonetheless, the simulation results were somewhat higher than those measured, which was most likely attributed to the following influencing factors: (a) all the bolts were taken as rigid and hence no deformation of the bolts was considered; (b) damping in various parts of the FE model (e.g., test specimen, bolt fixtures, support base, etc.) was not accounted for; and (c) the (tiny) clearance between screw and preformed hole on the beam/support/cushion block was not considered in FE simulation. How would these factors affect structural springback will be quantified in a separate study.

The numerically simulated dynamic response of the fully-clamped beam, especially contours of von Mises stress and distributions of maximum principal logarithmic strain, was presented in Fig. 8. For convenience, the surface of the beam hit directly by foam projectile was herein referred to as the "top" surface while the opposite surface was referred to as the "bottom" surface, as marked in Fig. 8a. It should also

**Fig. 7** Simulated mid-span deflection of fully-clamped beam plotted as a function of time. Experimentally measured peak deflection ($\delta_p$) and residual deflection ($\delta_r$) were also presented for comparison
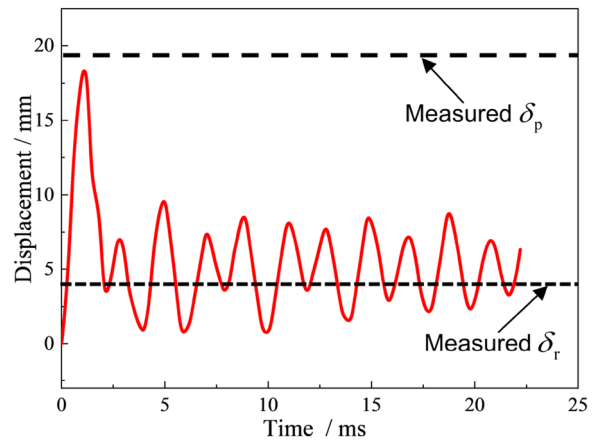
**Fig. 8** Temporal evolution of **a** von Mises stress and **b** maximum logarithm principal strain distribution along the axial central line of a fully-clamped steel beam
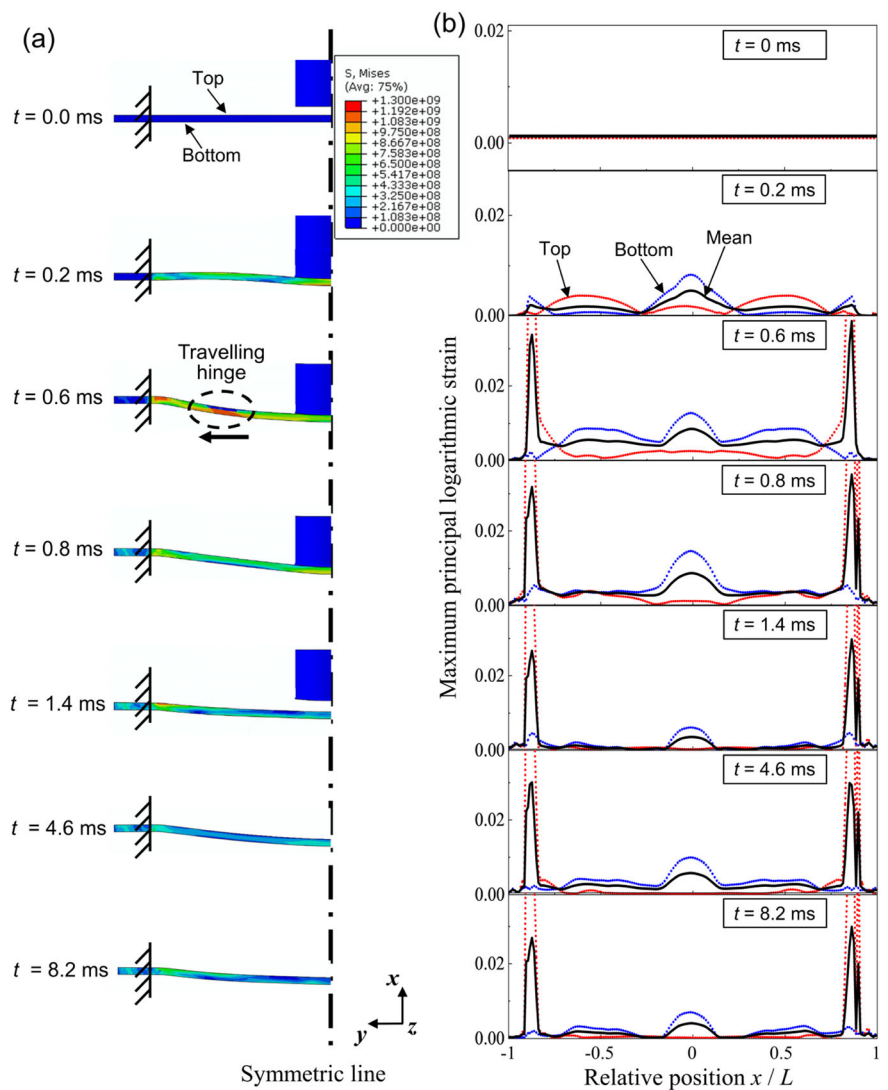
be pointed out that the curves of maximum principal logarithmic strain in Fig. 8b presented the strain distribution along the $y$-directional central line on the top surface (highlighted in red) and the corresponding one on the bottom surface (highlighted in blue). Another curve, the black one, presented the average of the red and blue curves. The variation trend of the Mises stress distribution (Fig. 8a) illustrated that, shortly after the impact ($t = 0.2$ ms), a localized region with higher stress (i.e., local hinge) appeared in the region directly hit by the projectile. Thereafter, this localized region (hinge) started to travel in the beam along both the positive and negative $y$-directions and, eventually (at about $t = 0.6$ ms), reached the clamped ends. Subsequently, the high stress region was mainly localized within the mid-span and the clamped end regions.

In accordance with the temporal evolution of Mises stress distribution displayed in Fig. 8a, at $t = 0.2$ ms, the maximum principal logarithmic strain was localized mainly within the mid-span region of the bottom surface and the quarter-span region of the top surface, as shown in Fig. 8b. In contrast, at this moment ($t = 0.2$ ms), the corresponding strains near the clamped ends of the beam were relatively small. Subsequently, however, at about $t = 0.6$ ms, the strain in the mid-span region of the bottom surface decreased, accompanied with increased strain in the quarter-span region of the bottom surface. Meanwhile, the intense strain in the unclamped region of the top surface moved to the distal end. Thereafter, the high strain regions were mainly located within two zones,

the mid-span of bottom surface and the two clamped ends of top surface. In addition, the black curve of Fig. 8b also elucidated the transferring of localized region having intense strain and the formation of stable region with relatively high strain. These results indicated that the phenomenon of traveling hinges occurred in the initial stage of impulsive impact and had limited influence on the permanent (residual) deflection of the beam.

Figure 9 plotted the numerically calculated kinetical energy, elastic deformation energy and plastic deformation energy of the whole beam as functions of impact time. Once the fully-clamped beam started to sustain the impulsive loading, its kinetic energy increased sharply, accompanied by a gentle rising of its deformation energy. Upon peaking, the kinetic energy dropped sharply, implying that the loading stage (via foam projectile) terminated and a subsequent transferring process of the kinetical energy into the deformation energy began. Particularly, during this transfer process of energy, the plastic deformation energy increased sharply and, upon reaching the stable stage ($t > 1.4$ ms), it became approximately equal to the peak of kinetic energy. This indicated that, during the stable stage, the elastic deformation energy faded gradually, and the plastic deformation energy stabilized to a constant close to the peak of kinetical energy. Notably, the loss of elastic deformation energy immediately after reaching the peak of kinetic energy led to the springback of the beam, which was the main focus of the analytical model proposed in the next section.

**Fig. 9** Temporal evolution of kinetical energy, elastic deformation energy and plastic deformation energy within the impulsively loaded armor steel beam
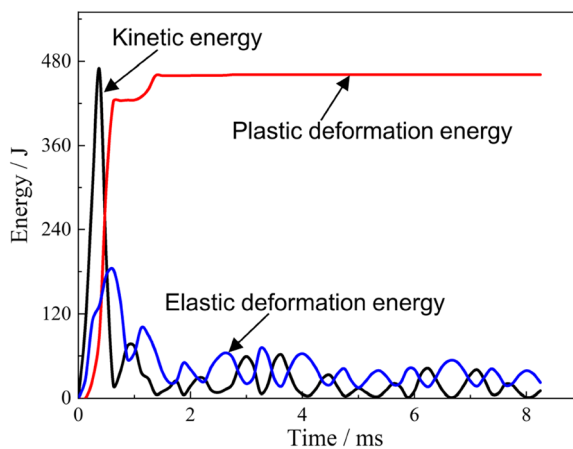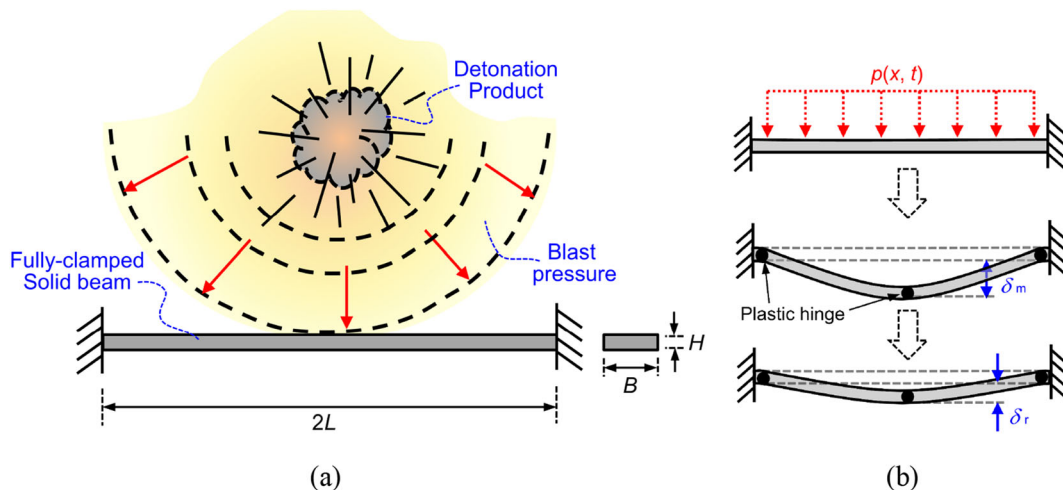
**Fig. 10** Schematic of **a** impulsive loading on a fully-clamped metallic beam and **b** structural responses of a fully-clamped metallic beam subjected to uniform areal impulsive load

## 4 An analytical model of springback

### 4.1 The three basic stages of springback

Based on experimental and numerical observations, the key features of springback in a metallic beam with fully-clamped edges were highlighted in this section. With reference to Fig. 10a, consider a fully-clamped beam subjected to a shock wave due to, say, detonation of shallow-buried explosives. The beam has length $2L$, width $B$ and thickness $H$. For simplicity, instead of the localized impulsive loading (via foam projectile) considered in the impact test of Sect. 2, the impulsive load generated by the blast was taken as an approximately uniform areal load with short duration (Fig. 10b) such that an analytical model of springback could be established.

Consistent with existing studies (e.g., Schleyer and Hsu 2000; Yuan et al. 2016; Tian et al. 2020), the experimental and numerical results presented hitherto demonstrated that the whole dynamic response of a structure loaded impulsively could be taken as consisted of three basic stages: the initial loading stage, the transient stage with the producing and merging of travelling plastic hinge(s), and the final stage with stationary hinges and deformation. Alternatively, the three basic stages could be termed as the load-imposing stage, the deforming stage, and the unloading stage (Shi et al. 2018), as shown schematically in Fig. 10b. During the first stage, the external

work of the pressure impulsive is transformed into equivalent kinetical energy within the loaded beam. Subsequently, structural deformation of the beam, including deflecting, stretching and rotating, takes place to absorb its kinetic energy. At the end of this stage, the beam arrests, and the transformation of kinetical energy to strain energy is complete. Critically at this moment, the beam reaches its peak deflection (labeled herein as $\delta_m$) at its center and, immediately after, unloading is initiated. During the unloading stage, structural deformation of the beam, especially within the elastically-dominated deformation regime, will be reduced or even vanish. Upon dissipating the elastic strain energy via structural damping and/or oscillation, permanent deflection of the beam is formed, labeled herein as $\delta_r$.

### 4.2 Basic assumptions

Based upon the three distinct stages of a dynamically loaded and fully-clamped metallic beam shown in Fig. 10b, an analytical model was established below to predict its springback response. To this end, the following basic assumptions were made:

- The beam is relatively thin and slender, and its cross-section remains plane and perpendicular to its longitudinal axis after stretching or bending.
- Stresses across the thickness of the beam are negligible, such that the stress is uniaxial (along the longitudinal axis) and uniform across the beam.

- Constant volume (conservation of mass) holds during the whole response process of the beam.
- The deformation theory of elastic-perfectly plasticity without strain hardening and strain rate effect holds, and no material fracture is considered.
- The loading duration of the transient impulse is much shorter than the response duration of the loaded beam.
- The static approach without considering traveling plastic hinges is suitable to derive analytical solutions of springback.

The last assumption about using the static approach in a dynamic problem needs further explanation. The main focus of the present study—springback of fully-clamped beam loaded impulsively—is dependent directly on the transient peak deflection and permanent residual deflection, which occur separately at the end of the transient stage and the final stage as illustrated in Fig. 10b. Under such conditions, the beam system satisfies the principle of energy conservation that is insensitive to time. Previous studies [e.g., Yu et al. 2018] suggested that, the final deformation mode of an impulsively loaded structure is usually similar to that associated with the elasto-plastic collapse mechanism found in the same structure but loaded quasi-statically. To avoid the daunting task of solving the kinetic equilibrium equations by considering plastic hinge(s) that travel in the beam, the springback of an impulsively loaded beam may be approximately taken as independent of time and solved using an (approximate) static method as done in the current study. In addition, a recent study [Tian et al. 2020] on a dynamically loaded square plate reported a negligible difference between analytical predictions obtained with and without considering travelling plastic hinges. Hence it is considered acceptable to develop analytical solutions of springback by using a static approach without considering traveling plastic hinges.

Under the forgoing assumptions, the longitudinal total strain of the beam may be written as:

$$\varepsilon = \varepsilon_e + \varepsilon_p \tag{2}$$

where $\varepsilon_e$ is the elastic strain and $\varepsilon_p$ is the plastic strain. For pure elastic deformation, Hooke's law is satisfied. For simplicity, when the material enters plastic yielding, a constant yielding stress, without strain hardening, was assumed. (The effects of strain hardening as well as strain rate were quantified in

Sect. 5.2 with FE simulations.) Thus, the constitutive model for ideal elastic–plastic deformation could be expressed as:

$$\sigma = f(\varepsilon) = \begin{cases} E\varepsilon, \, \varepsilon \le \varepsilon_e \\ \sigma_y, \, \varepsilon \ge \varepsilon_e \end{cases}. \tag{3}$$

where $E$ is the Young's modulus, $\sigma_y$ is the yield strength, and $\varepsilon_y$ is the corresponding yield strain of the material make of the beam.

### 4.3 Analytical solution of springback

#### 4.3.1 Loading status and deflection profile

As previously mentioned, the dynamic response of a fully-clamped metallic beam can be divided into the loading, deforming and unloading stages of Fig. 10b. Correspondingly, its temporal structural response looks like the one shown schematically in Fig. 11a, with representative status in each stage clearly marked: *Status I* representing the end of the loading stage, *Status II* where beam deflection reaches a peak during the deforming stage, and *Status III* where beam deflection becomes permanent at the end of the unloading stage. To analytically characterize the key features of springback, the beam was conveniently modeled using a beam-hinge system (Schleyer and Hsu 2000), as shown in Fig. 11b. Built upon this beam-hinge system, Fig. 11c depicted schematically the deformation mode of the beam corresponding to each status marked in Fig. 11a.

Due to the typically short duration of impulsive loading (Fig. 11a), it was assumed that the loaded beam obeys the following impulse conservation:

$$p(t,x)t = \mu v(t,x) \tag{4}$$

where $p$ is the loading pressure, $\mu$ is the areal density of the beam, and $v$ is the velocity of material element in the beam.

Note that, at *Status I*, the loading period of the transient impulse is typically much shorter than the duration of the structural response (Jones 2000). It was then assumed that deformation was initiated in the beam immediately after the impact took place, and its kinetic energy $E_k$ transferred from the external impact work could be calculated as:

**Fig. 11 a** Typical temporal response of a fully-clamped metallic beam under dynamic load, **b** beam-hinge system of the beam, and **c** schematic of deformation modes corresponding to the marked statuses in **a**
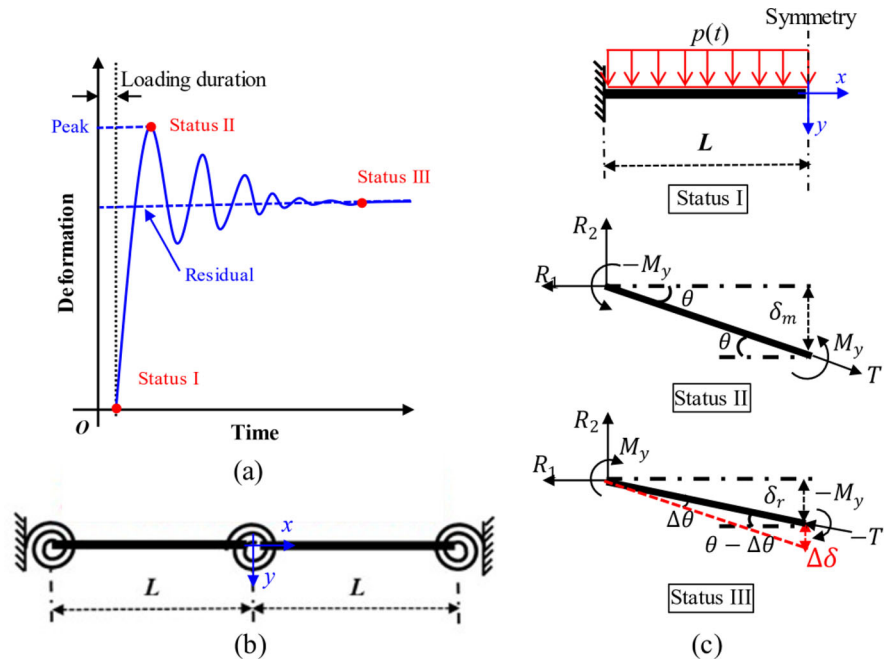


$$E_k = \frac{1}{2} \int_0^L \mu A v^2 dx \tag{5}$$

Meanwhile, conservation of energy dictates that, at either *Status II* or *Status III*, $E_k = U$ where $U$ is the deformation energy (internal energy) of the beam.

During the deformation stage (between *Status I* and *Status II*), the transverse deflection (displacement) as well as the velocity of a beam element at axial location $x$ were assumed to exhibit a linear triangular profile, as (Jones 2000):

$$\delta(x) = W(1 - \frac{x}{L}) \tag{6}$$

$$v(x) = V(1 - \frac{x}{L}) \tag{7}$$

where $W$ and $V$ denote the transverse deflection and velocity at beam center.

At *Status II*, the central point of the beam reaches the maximum (peak) deflection $\delta_m$ while its velocity drops to zero (i.e., $V = 0$). At this moment, the kinetic energy $E_k$ of the beam is completely converted into the deformation energy $U$. In the present study, it was assumed that the deformation energy is composed of two components, $U = U_t + U_m$, where $U_t$ is induced by membrane force in the axial direction and $U_m$ by rotation of the hinges. Thus, with $T$ and $M$ denoting the

axial force and bending moment at location $x$, respectively, one has:

$$U = \int \frac{T^2}{EA} dx + \int \frac{M^2}{EI} dx \tag{8}$$

When a beam element enters plastic yielding, the axial force acting on the element becomes $T_y = \sigma_y BH$ and the bending moment becomes $M_y = \sigma_y BH^2/4$.

According to the magnitude of kinetic energy $E_k$ and the key deformation features of a fully-clamped metallic beam, three distinct cases were identified for subsequent analytical modeling. One extreme case is when $E_k$ is too small to induce any plastic deformation within the beam such that only elastic deformation contributes to its deformation energy. Consequently, in the absence of plastic deformation, the beam exhibits no residual (permanent) deflection when the loading is complete. This particular case was not considered in the current study. Another extreme case is when the kinetic energy $E_k$ is too large that the entire beam becomes plastically yielded, both in axial stretching and rotation. Correspondingly, plastic deformation dominates the deformation energy and hence springback of the beam. The third is an intermediate case: the beam is elastically stretched in the axial direction but plastically rotated at the hinges: as a result, its springback behavior is dominated by

elastic deformation. The latter two cases were analyzed in detail below.

### 4.3.2 Springback dominated by elastic deformation

In this circumstance, at *Status II*, the beam does not undergo plastic deformation except at the two ends and the center where plastic hinges are formed. It follows that while the three hinges are plastically yielded via rotation, the tensile deformation energy $U_t$ of the beam is contributed solely by elastic deformation via axial stretching. Correspondingly, the plastic deformation energy $U_m$ of the beam contributed solely by the hinges is:

$$U_m = 4M_y\theta_m \tag{9}$$

For slender beams considered herein, $\delta_m \ll L$ holds such that the peak rotation angle $\theta_m$ can be approximated as:

$$\theta_m = \arctan\left(\frac{\delta_m}{L}\right) \approx \frac{\delta_m}{L} \tag{10}$$

The deformation energy $U_t$ induced by axial tensile deformation is:

$$U_t = 2\frac{T^2 L}{EA}\left(\sqrt{1 + \left(\frac{\delta_m}{L}\right)^2} - 1\right) \tag{11}$$

where $T = EA\left[\sqrt{1 + \left(\frac{\delta_m}{L}\right)^2} - 1\right]$ denotes the axial tensile force at the moment when the beam reaches its maximum deflection $\delta_m$. At this moment (i.e., *Status II*), as previously mentioned, the deformation velocity of the beam drops to zero. Energy conservation then dictates:

$$E_k = 4M_y\frac{\delta_m}{L} + 2\frac{T^2}{EA}L\left[\sqrt{1 + \left(\frac{\delta_m}{L}\right)^2} - 1\right] \tag{12}$$

Substituting the axial tensile force $T$ into Eq. (12) gives:

$$E_k = 4M_y\frac{\delta_m}{L} + 2EAL\left[\sqrt{1 + \left(\frac{\delta_m}{L}\right)^2} - 1\right]^3 \tag{13}$$

With $\delta_m \ll L$ (i.e., $\frac{\delta_m}{L} \to 0$) assumed for slender beams, Eq. (13) can be simplified as:

$$E_k \approx 4M_y\frac{\delta_m}{L} + \frac{1}{4}EAL\left(\frac{\delta_m}{L}\right)^6 \tag{14}$$

The peak deflection $\delta_m$ can then be calculated from the foregoing equation.

At *Status III*, the elastic deformation energy $U_e$ stored within the beam causes it to spring back from its peak deflection. Such springback leads to decreased tensile deformation in axial direction, reduced beam deflection, and converse rotation of plastic hinges. Correspondingly, energy conservation requires:

$$U_e = EAL\Delta\varepsilon^2 + 4M_y\Delta\theta \tag{15}$$

where $\Delta\varepsilon \approx \frac{\Delta\delta}{L^2}\left(\delta_m - \frac{\Delta W}{2}\right)$ is the decreased axial strain, and $\Delta\theta \approx \frac{\Delta\delta}{L}$ is the reduced rotation, $\Delta\delta = \delta_m - \delta_r$ being the magnitude of springback (measured at beam center; Fig. 10b). Equation (15) can be rewritten as:

$$U_e = 2EA\frac{\Delta\delta}{L}\left(\delta_m - \frac{\Delta\delta}{2}\right) + 4M_y\frac{\Delta\delta}{L} \tag{16}$$

from which:

$$\Delta\delta = \frac{4M_y + 2EA\delta_m + \sqrt{(4M_y + 2EA\delta_m)^2 - 4EALU_e}}{2EA} \tag{17}$$

here $U_e$ is the elastic deformation energy induced by axial tensile force at *Status II*, given by:

$$U_e = U_t - 2\theta M_y \tag{18}$$

### 4.3.3 Springback dominated by plastic deformation

In this case, the beam has a sufficiently large kinetic energy $E_k$ such that the entire beam enters the fully plastic stage. The axial tensile deformation energy is thus comprised of fully plastic deformation energy, given as:

$$U_t = 2\frac{T_y^2}{EA}L\left(\sqrt{1 + \left(\frac{\delta_m}{L}\right)^2} - 1\right) \approx \frac{T_y^2\delta_m^2}{EAL} \tag{19}$$

where $T_y$ is the critical axial tensile force corresponding to the moment when the entire beam is fully yielded. At *Status II*, energy conservation requires:

$$E_k = 4M_y \frac{\delta_m}{L} + 2T_y L \left[ \sqrt{1 + \left(\frac{\delta_m}{L}\right)^2} - 1 \right] \quad (20)$$

Solving Eq. (20) leads to the following maximum beam deflection:

$$\delta_m = \frac{\sqrt{E_k^2 L^4 T_y^2 + 16 L^4 M_y^2 T_y^2 + 4 E_k L^5 T_y^3} - 2E_k L M_y - 4L^2 M_y T_y}{2(L^2 T_y^2 - 4M_y^2)}$$
$$(21)$$

which, with small deformation assumed, can be simplified as:

$$\delta_m \approx \frac{\sqrt{4M_y^2 + LT_y E_k} - 2M_y}{T_y} \quad (22)$$

Consider next *Status III*. At this moment, the axial tensile deformation energy $U_t$ is comprised of two components, $U_t = U_{te} + U_{tp}$, where the elastic deformation energy $U_{te}$ (Gauch et al. 2018) and the plastic deformation energy $U_{tp}$ (Schleyer and Hsu 2000) are given by:

$$U_{te} = 2\frac{\Delta L_p^2 EA}{L} = 2EA\varepsilon_y^2 L \quad (23)$$

$$U_{tp} = U_t - U_{te} \quad (24)$$

here $\Delta L_p$ is the critical tensile displacement of the beam (along its axial direction) when it reaches the fully plastic stage. On the other hand, due to conservation of energy, the total energy $U_e$ of the beam governed by converse axial deformation $\Delta\varepsilon$ and converse rotation $\Delta\theta$ is given by:

$$U_e = 2\sigma_y A \Delta L_p + 4M_y \Delta\theta \quad (25)$$

Given that $U_{te} = U_e$, Eq. (24) can be rewritten as:

$$U_e = 2T_y \frac{\Delta\delta}{L}\left(\delta_m - \frac{\Delta\delta}{2}\right) + 4M_y \frac{\Delta\delta}{L} \quad (26)$$

from which:

$$\Delta\delta = \frac{(4M_y + 2\delta_m T_y) - \sqrt{(4M_y + 2\delta_m T_y)^2 - 4T_y L U_e}}{2T_y}$$
$$(27)$$

Finally, the residual deflection $\delta_r$ at beam center (Fig. 11b) is given by:

$$\delta_r = \delta_m - \Delta\delta \quad (28)$$

The springback $\Delta\delta$ of the beam can be expressed in a dimensionless way, as:

$$\Delta\overline{\delta} = \frac{\Delta\delta}{L} \quad (29)$$

## 5 Results and discussion

In this section, a systemic study of springback in an impulsively loaded and fully-clamped metallic beam was performed, both analytically and numerically. To explore the physical mechanisms underlying springback, three steel alloys, one aluminum alloy and one titanium alloy were purposely selected for illustration. The three steels have nearly identical density ($\sim 8000$ kg/m$^{-3}$) and elastic modulus ($\sim 200$ GPa), but vastly different yielding strength (205 MPa for 304 SS, 819 MPa for Weldox 700E, and 1372 MPa for Armox 500 T).

### 5.1 Effect of yield strength

To quantify the effect of yield strength on springback, predictions obtained by using the proposed analytical model were firstly compared with FE simulation results for fully-clamped beams made of three representative steels: 304 SS, Weldox 700E and Armox 500 T. Table 2 listed relevant material parameters collected from previous studies (Xue and Hutchinson 2004; Iqbal et al. 2016; Zakrisson et al. 2011). For both analytical modeling and FE simulation, the three steels having similar densities and Young's moduli but significantly different yielding strengths were all assumed to obey the elastic-perfectly plastic constitutive model, with plastic strain hardening and strain rate effect excluded. Later, these limits were relaxed, as detailed in subsequent sections.

The normalized beam deflection $\delta/L$(left figures) and normalized springback $\Delta\delta/L$(right figures) were plotted in Fig. 12a–c as functions of beam kinetic energy $E_k$ for 304 SS, Weldox 700E and Armox 500 T, respectively. Analytical model predictions and FE simulation results were both presented and compared. Overall, for each type of steel, reasonable agreement was achieved for the considered range of $E_k$, thus validating to a certain extent the analytical model developed in the current study.

**Table 2** Material parameters of selected steels

| Steel type | 304 SS | Weldox 700E | Armox 500 T |
|---|---|---|---|
| Density (kg/m$^3$) | 8000 | 7850 | 7850 |
| Young's Modulus (GPa) | 210 | 210 | 200 |
| Yield Strength (MPa) | 205 | 819 | 1372 |
| Reference | Xue and Hutchinson (2004) | Zakrisson et al. (2011) | Iqbal et al. (2016) |

It was seen from Fig. 12a that, for 304 SS having a relatively low yield strength, the analytically predicted values of $\delta/L$, including peak deflection $\delta_m/L$ and permanent deflection $\delta_r/L$, were slightly smaller than those numerically calculated within the elasticity-dominated stage, but agreed well with the latter within the plasticity-dominated stage. Similarly, for Weldox 700E having a moderate yield strength, the results of Fig. 12b demonstrated good agreement between analytical and numerical results, especially for beam deflection; further, the peak value of $\Delta\delta/L$ was well captured by the analytical model. In contrast, for Armox 500 T that has a relatively high yield strength, the analytical predictions of $\delta_m/L$ and $\delta_r/L$ were both distinctively smaller than their numerical counterparts, especially within the intermediate zone between elasticity- and plasticity-dominated stages (Fig. 12c). This was understandable, given that the analytical model did not consider the springback performance in the intermediate zone where both elastic deformation and plastic deformation play significant roles in beam deflection. Nonetheless, the difference between $\delta_m$ and $\delta_r$ (i.e., springback $\Delta\delta$) was well predicted by the analytical model, as shown in Fig. 12c.

As the initial kinetic energy ($E_k$) of the beam was increased, its springback $\Delta\delta$ exhibited distinct variation trend, as shown in Fig. 12. Regardless of steel type, the value of $\Delta\delta$ sharply increased with increasing $E_k$, and the rate of increase slowed down as the peak of $\Delta\delta$ was reached; when $E_k$ was further increased, the springback $\Delta\delta$ gradually decreased. The increasing stage of $\Delta\delta$ corresponded to the elasticity-dominated stage, while the decreasing stage after the peak corresponded to the plasticity-dominated stage. At the joint of the two stages, especially where the beam reached its peak deflection, the kinetic energy was equal approximately to the threshold of elastic deformation energy that could be stored in the beam.

Consequently, for a given material make, the peak springback of the beam was dependent upon two key factors: the kinetic energy imposed by the impulse load and the threshold of elastic deformation energy stored in the beam. Among the three steel types considered, 304 SS with the lowest yield strength required $E_k = 0.8\,kJ$ to reach the peak springback (Fig. 12a), while the corresponding $E_k$ for the high strength Armox 500 T was 15.2 kJ (Fig. 12a). That is, for the case investigated in the current study, when the yield strength was enhanced by 6.7 times (from 205 to 1372 MPa), the initial kinetic energy inducing a peak springback required a 19 times increase. Correspondingly, the peak $\Delta\delta$ for the Armox 500 T beam was increased by 1.8 times relative to the 304 SS beam. This result revealed that the beam made of a higher yield strength metal would exhibit a higher springback when impulsively loaded, thus requiring more caution in the practical design of protective structures made of high strength metallic materials.

The analytical and numerical results of Fig. 12 demonstrated clearly that the springback performance of a fully-clamped steel beam is dependent strongly upon the yield strength of its material make, governed by storing and releasing of elastic strain energy in the beam. Thus, during the dynamic loading process, the variation of internal potential energy brings a great difference in springback (Shi et al. 2018). Consequently, the analytical model was employed to explore further the influence of yield strength on springback, for fully-clamped beams made of steels having different yield strengths but identical mass density and Young's modulus. To this end, a dimensionless parameter $\eta = \sigma_{y0}/\sigma_0$ was introduced, where $\sigma_0$ denotes the yield strength of 304 SS steel (taken here as reference) and $\sigma_{y0}$ is the yield strength of alternative steel, such as Weldox 700E and Armox 500 T listed in Table 2. In addition, it was assumed that when the
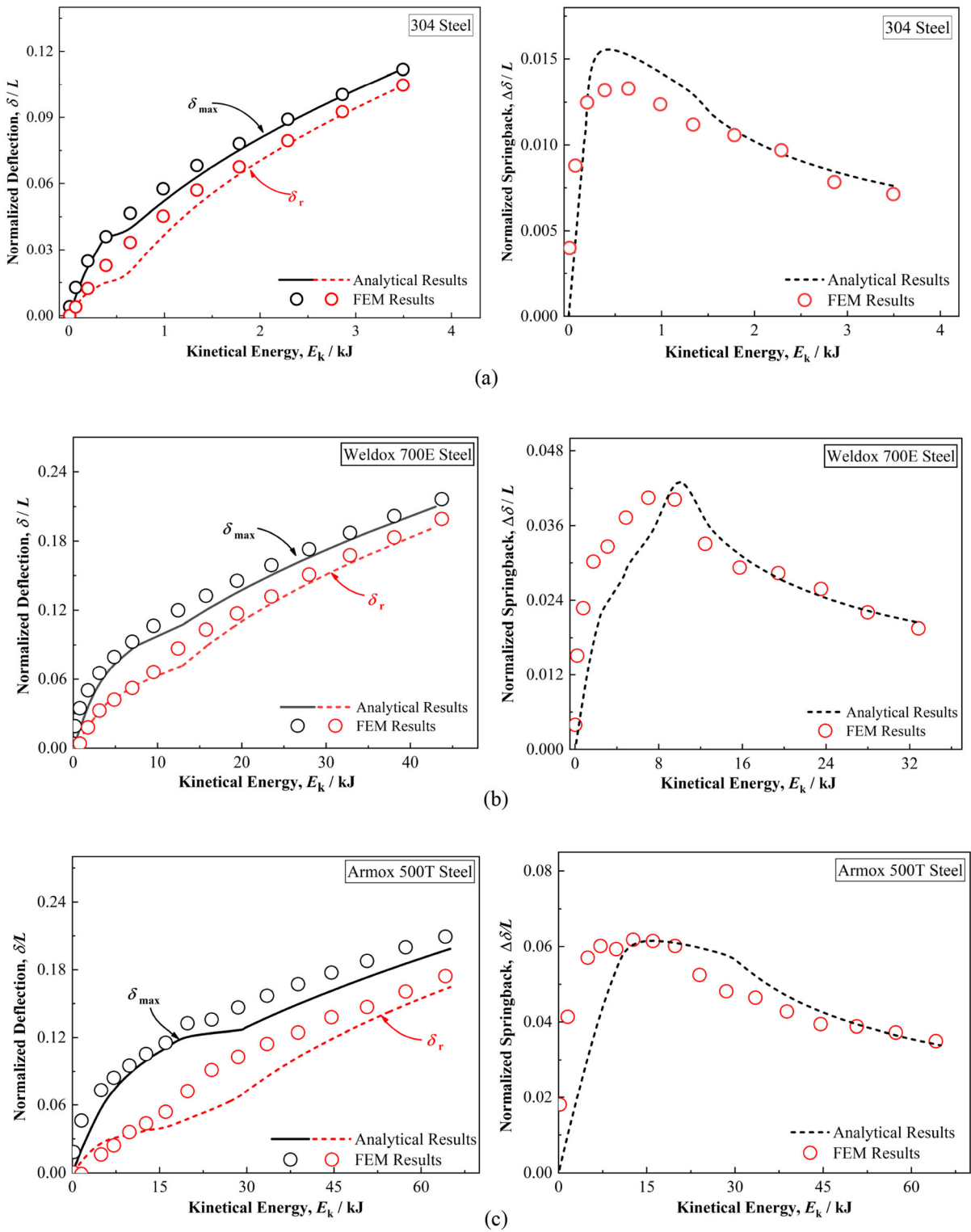
Fig. 12 Comparison between analytically predicted and numerically calculated beam deflections (left) and springbacks (right) for a fully-clamped beam made of **a** 304 SS, **b** Weldox 700E and **c** Armox 500 T

**Fig. 13 a** Peak elastic strain energy stored in a fully-clamped steel beam plotted as a function of dimensionless impulse and **b** ratio of elastic strain energy to plastic strain energy (left) and ratio of elastic strain energy to internal potential energy (right), for selected values of yield strength ratio $\eta$
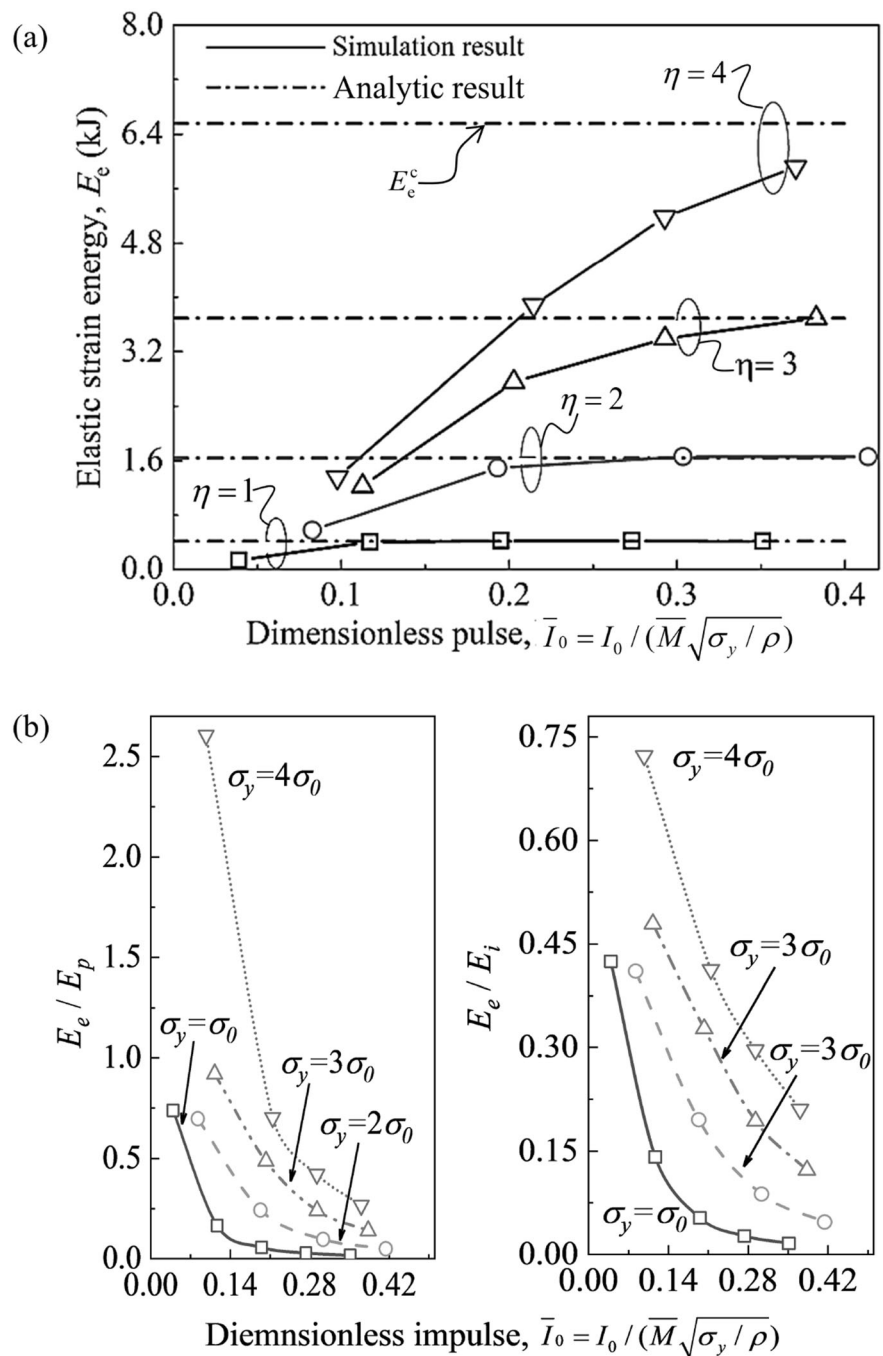
entire beam is plastically yielded, the elastic deformation energy stored within the beam is fully consumed by plastic deformation. This critical elastic deformation energy was designated herein as the threshold of elastic strain energy ($E_e^c$) that can be stored by the beam, calculated as:

$$E_e^c = \iiint_V \sigma_e \varepsilon_e dV = \frac{\sigma_0^2 V}{2E} // 0 \leq \sigma_e \leq \sigma_0 \qquad (30)$$

where $\sigma_e$ is the elastic stress, $\varepsilon_e$ is the corresponding strain and $V$ denotes the total deforming volume of the beam.

The peak elastic deformation energy stored in the fully-clamped beam was plotted in Fig. 13a as a function of dimensionless impulse $\bar{I}_0$ for selected values of yield strength ratio $\eta$. As $\bar{I}_0$ was increased, the peak elastic deformation energy increased and approached gradually to its threshold $E_e^c$, the latter strongly dependent upon $\eta$. It was seen that when the beam was made of a lower yield strength steel (thus a smaller $\eta$), it was easier for its elastic deformation energy to approach the threshold. In other words, with $\bar{I}_0$ fixed, the beam having a smaller $\eta$ exhibited a larger deflection. For the case considered here, when the yield strength ratio was increased from $\eta$ to $\eta = 2$ and $\eta = 3$, the threshold of impulse load causing the elastic deformation energy to reach $E_e^c$ was correspondingly increased from $\bar{I}_0 = 0.11$ to 0.31 and 0.38. If the beam was made of a steel with $\eta = 4$, the critical (dimensionless) impulse corresponding to $E_e^c$ exceeded 0.5, as could be seen from Fig. 13a.

In Fig. 13b, the ratio of elastic deformation energy to the corresponding plastic deformation energy, $E_e/E_p$, and the ratio of elastic deformation energy to the corresponding internal potential energy, $E_e/E_i$, were both plotted as functions of $\bar{I}_0$ for selected values of $\eta$. Due to the threshold of elastic deformation energy stored in a fully-clamped beam, there exists a limit on the amount of kinetic energy converted to elastic deformation energy. When the elastic deformation energy reaches its threshold $E_e^c$, plastic deformation becomes the only route to covert the remaining kinetic energy into internal potential energy. Overall, as shown in Fig. 13b, the energy ratios $E_e/E_p$ and $E_e/E_i$ decreased as $\bar{I}_0$ was increased, and the decline was more significant when $\eta$ had a smaller value. This was attributed to the fact that, with $\bar{I}_0$ fixed, the beam with a higher yield strength had a greater capacity to store elastic deformation energy.

To explore the variation trend of springback with varying composition of internal energy, Fig. 14 plotted $\Delta\delta/L$ as a function of $E_e/E_p$ for selected values of yield strength ratio $\eta$. The results of Fig. 14 revealed that (1) $\Delta\delta/L$ first increased and then fell as $E_e/E_p$ was increased, and (2) with $E_e/E_p$ fixed, $\Delta\delta/L$ increased with increasing $\eta$. Besides, each $\Delta\delta/L$ versus $E_e/E_p$ curve exhibited two distinct regimes. The first regime, lying on the left of peak $\Delta\delta/L$, was dominated by plastic deformation. Within this regime, the springback increased as the elastic strain energy stored
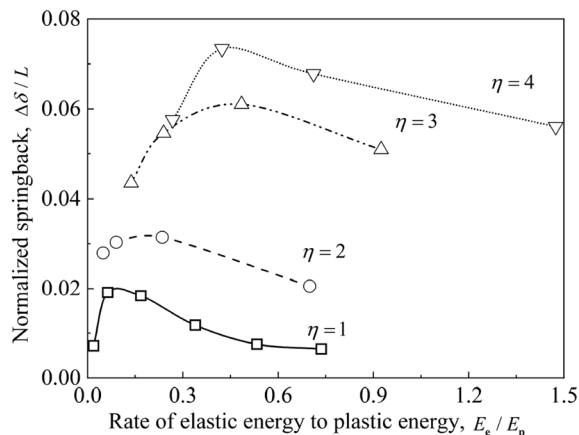


**Fig. 14** Normalized springback plotted as a function of the ratio of elastic strain energy to plastic energy for selected values of yield strength ratio $\eta$

within the impulsively loaded beam was increased. The second regime, on the right of peak $\Delta\delta/L$, was dominated by elastic deformation, with beam springback decreasing gradually as $E_e/E_p$ was increased. It should be mentioned that the elasticity-dominated stage corresponded to a relatively weak impulsive, while the plasticity-dominated stage corresponded to a significantly stronger impulse. Further, in terms of the changing slope of $\Delta\delta/L$, it was found that $\Delta\delta/L$ dropped more sharply within the plasticity-dominated stage. This explained why springback was more likely to be observed in a dynamically loaded beam made with a high yield strength metal. On the other hand, from Fig. 14 it was seen that for the beam having a smaller $\eta$, its peak $\Delta\delta/L$ was smaller than that of the beam having a larger $\eta$. Therefore, to design a protective structure with enhanced springback resistance, it is preferable to select a metallic material with excellent plastic deformation capacity or low elastic strain energy threshold.

## 5.2 Effect of strain hardening and strain rate

As previously stated, the analytical model of springback was developed under the premise that the fully-clamped beams were made of ideal elastoplastic metals without strain hardening and rate effects. In this section, to quantify how springback was affected by strain hardening and strain rate, FE simulations were carried out. The material make of the clamped beam was assumed to satisfy the Johnson–Cook
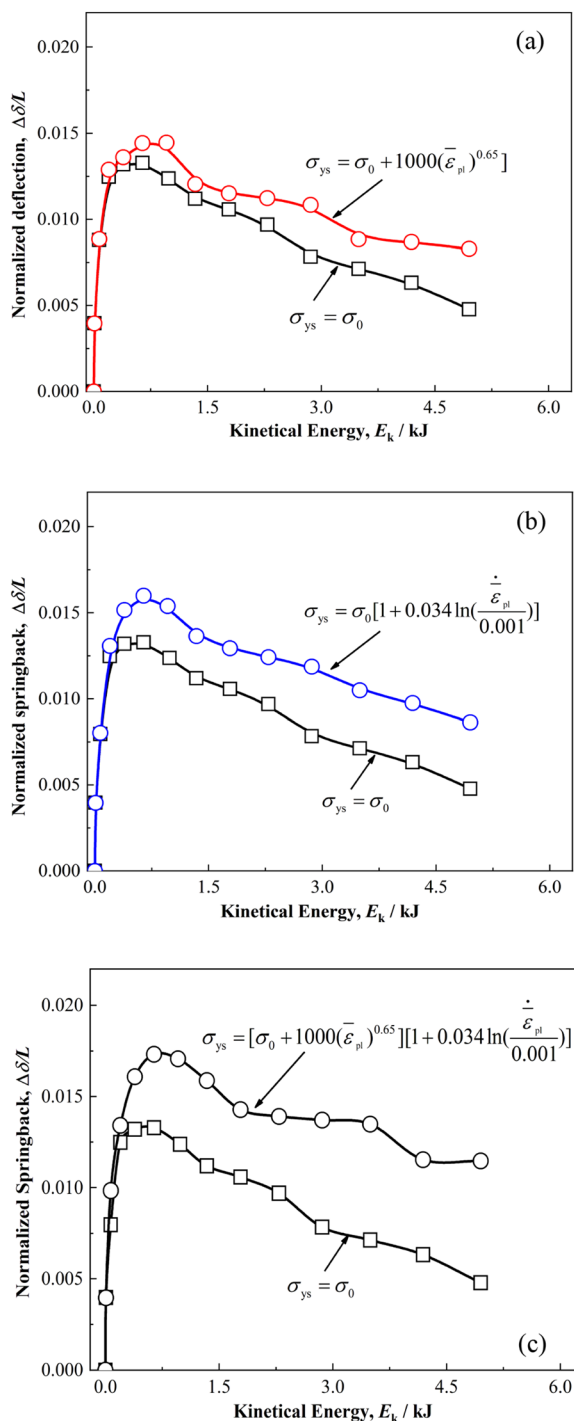
**Fig. 15** Influence of **a** strain hardening, **b** strain rate, and **b** combined effect of strain hardening and strain rate on springback of fully-clamped beam made of 304 stainless steel

plasticity model. For illustration, 304 stainless steel was selected, with $B = 1000$ MPa, $n = 0.65$, $C = 0.034$ and $\dot{\varepsilon}_0 = 0.001$ (Nahshon et al. 2007). The effects of strain hardening alone, strain rate alone, and combined strain hardening and strain rate on springback were separately quantified with FE simulations. For comparison, the case analyzed in the previous section without considering strain hardening and strain rate effects was taken as benchmark. The results thus calculated were presented in Fig. 15, with the benchmark case marked by hollow squares ($\square$).

The results of Fig. 15 revealed that both strain hardening and strain rate led to significantly enhanced springback ($\Delta\delta/L$) relative to the benchmark case, either acting separately or together, except for the elasticity-dominated stage (i.e., the increasing stage of each curve) where such effects were negligible. As an example, while the ideal elastoplastic beam (i.e., the benchmark) reached its peak springback of $\Delta\delta/L = 0.0133$ at $E_k = 0.64$ kJ, the corresponding $\Delta\delta/L$ value was 0.014 if strain hardening was considered, 0.016 if strain rate considered, and 0.017 if both considered. This indicated that the springback of a fully-clamped metallic beam is intensified if the strength of its material make is enhanced by strain hardening and strain rate, particularly so when its kinetical energy acquired from the loading impulse is sufficiently large.

To better understand the enhanced springback shown in Fig. 15, with the kinetic energy fixed at $E_k = 0.64$ kJ, the dynamic responses were compared between two selected cases: the benchmark and the case with combined effect considered. Corresponding results were presented in Fig. 16a in terms of $\Delta\delta/L$ and $E_e$ varying with time. Compared to the benchmark, the beam with combined effect considered possessed a lower $\Delta\delta/L$ and a higher $E_e$, including the peak and subsequent values as time passed by. This suggested that material strengthening due to strain hardening and strain rate effects contributed to significantly enhanced loading capacity and storage of elastic deformation energy.

For both cases, Fig. 16b presented the distributions of stress and logarithmic strain in an impulsively loaded beam at the moment when it reached peak deflection. Compared to the benchmark case, the consideration of both strain hardening and strain rate

**Fig. 16 a** Temporal evolution of springback $\Delta\delta/L$ (upper) and elastic strain energy $E_e$ (below) of a fully-clamped 304 SS steel beam with and without considering strain hardening and strain rate effects, and **b** distributions of strain and stress when the beam of **a** reached peak deflection. For both plots, $E_k = 0.64$ kJ



$$\sigma_{ys} = \sigma_0$$

$$\delta_m/L$$

$$\sigma_{ys} = [\sigma_0 + 1000(\bar{\varepsilon}_{pl})^{0.65}][1 + 0.034\ln(\frac{\dot{\bar{\varepsilon}}_{pl}}{0.001})]$$

$$\sigma_{ys} = [\sigma_0 + 1000(\bar{\varepsilon}_{pl})^{0.65}][1 + 0.034\ln(\frac{\dot{\bar{\varepsilon}}_{pl}}{0.001})]$$

$$\sigma_{ys} = \sigma_0$$

(a)

Symmetrical

$$\bar{\varepsilon}_{pl,\,max} = 0.022 \qquad \bar{\varepsilon}_{pl,\,max} = 0.014$$

$$\sigma_{max} = 240 \text{ MPa} \qquad \sigma_{max} = 320 \text{ MPa}$$

Ideal elastoplastic 304 SS steel

304 SS steel with strain hardening and strain rate effect

(b)
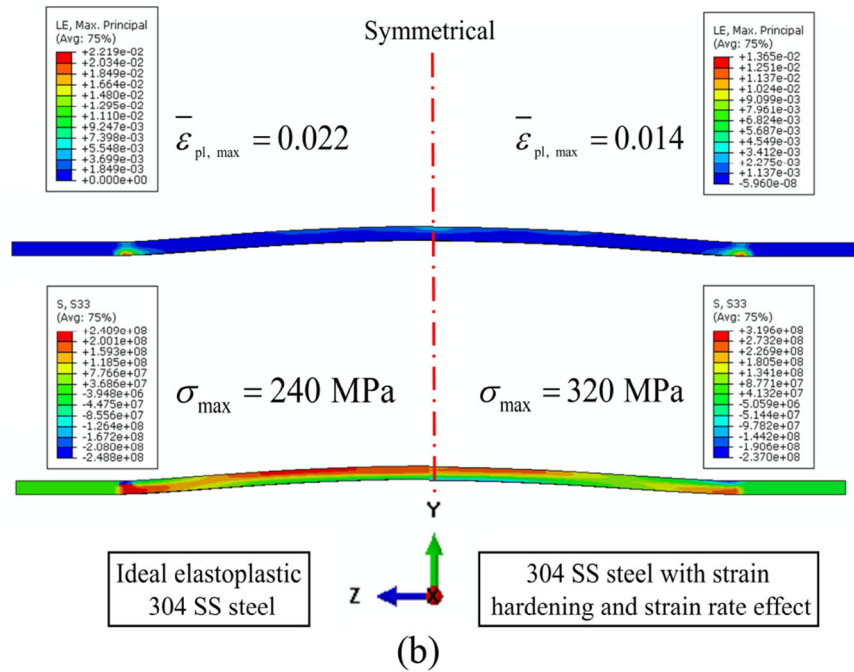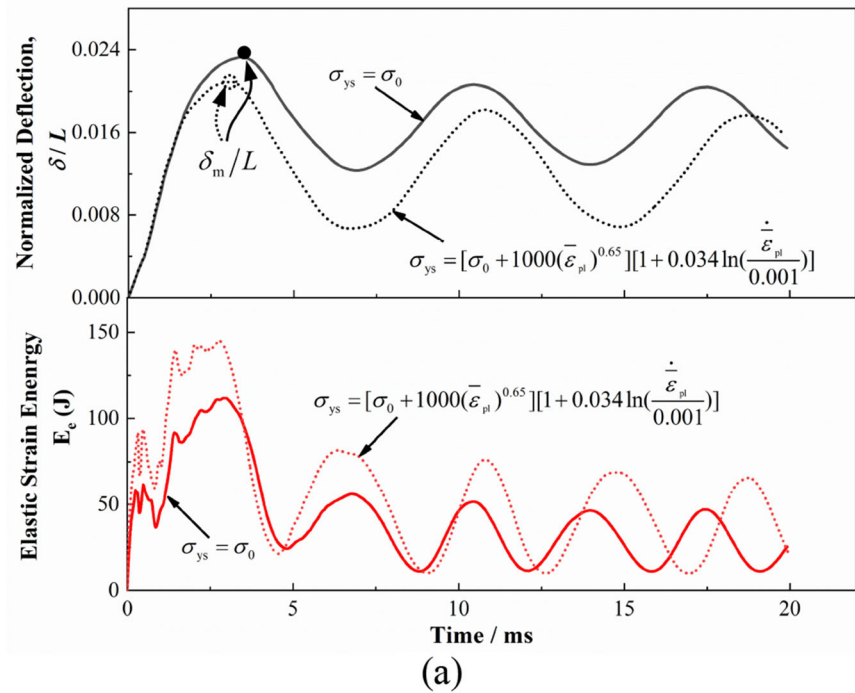
brought about a significant reduction in peak logarithmic strain and considerable enlargement in stress.

In summary, strain hardening and strain rate acted to increase the stress experienced by the beam once plastic deformation was initiated in the beam.

Accompanied by the enhanced yield strength of its material make, more stored deformation energy brought about a stronger potential of its springback. A higher yield strength also meant a higher loading capacity and hence a smaller peak deflection. All in

**Table 3** Material parameters of aluminum and titanium alloys

| Metal type | Al 5052-H38 | Ti-6Al-4 V |
|---|---|---|
| Density (kg/m$^3$) | 2680 | 4428 |
| Elastic Modulus (GPa) | 70 | 113.8 |
| Yield Strength (MPa) | 259 | 1098 |
| Reference | Khodaei et al. (2011) | Yuan et al. (2021) |

all, significantly enhanced springback occurred compared to the benchmark case.

## 6 Effect of springback on practical design of protective structures

In the previous section, the analytical model was first validated against FE simulation results and then employed to quantify the influence of yield strength on springback; subsequently, further FE simulations were carried out to investigate how strain hardening and strain rate affect springback, as both were neglected by the proposed analytical model. Nonetheless, the results were hitherto restricted to fully-clamped beams made of steel having identical density and elastic modulus. In the current section, the analytical model was employed to illustrate the importance of accounting for springback effect in the practical design of protective structures against impulsive blast loading. To this end, in addition to varying the yield strength, fully-clamped beams made of aluminum and titanium alloy were firstly considered. Relative to steel, these metals have significantly reduced density and elastic modulus, as shown Table 3 for Al 5052-H38 (density 2680 kg/m$^{-3}$ and elastic modulus 70 GPa) and Ti-6Al-4 V (density 4428 kg/m$^{-3}$ and elastic modulus 113.8 GPa).

With the effects of strain hardening and strain rate both ignored, Fig. 17a and b presented analytical and FE results for the aluminum beam and the titanium beam, respectively. The springback responses of both aluminum and titanium beams were seen to be similar to steel beams detailed in the previous section. Again, good agreement between analytical and FE results for both peak deflection and springback was achieved, thus further validating the proposed analytical model.

Next, to illustrate why springback should be accounted for in practical design of protective structures, the ratio of peak springback to residual (permanent) deflection ($\Delta\delta/\delta_r$) was plotted in Fig. 18 as a function of the ratio of kinetic energy to the threshold of stored elastic energy ($E_k/U_{te}$) for four different metals: 304 stainless steel, Armox 500 T steel, aluminum Al 5052-H38 and titanium Ti-6Al-4 V. To simplify the analysis of obtained results, the effects of strain hardening and strain rate were not accounted for. Here, the geometries of the beams made with different metals were identical to those described in Section 4.

In Fig. 18, the hollow symbols represented $\Delta\delta/\delta_r$ values obtained by FE simulations, while the dashed lines denoted envelop curves for these $\Delta\delta/\delta_r$ values.

For each of the 4 metal types considered, as $E_k/U_{te}$ was increased, $\Delta\delta/\delta_r$ increased first, reached a peak, followed by a sharp drop, and then gradually decreased. The peak of $\Delta\delta/\delta_r$ occurred approximately at $E_k/U_{te} = 1$, where the gap between peak deflection $\delta_m$ and permanent deflection $\delta_r$ was the largest. Accordingly, for practical applications, this may misguide the design of a protective structure if its impact resistance is evaluated in terms of its permanent deflection, rather than its transient peak deflection that is often difficult to observe during the process of impulsive loading, let alone measure it.

As shown in Fig. 18, among the 4 types of material make, the high-strength steel Armox 500 T exhibited the most significant springback, while the low-strength 304 SS had the least springback. Meanwhile, the large envelope region indicated that springback was significant and hence should not be ignored in not only practical design of a protective structure, but also assessment of its impact performance. Ideally, the protective structure should possess high impact resistance (low permanent deflection $\delta_r$) as well as good predictability of impact resistance (low springback $\Delta\delta$). It is therefore of interest and importance to consider both factors in protective designs.
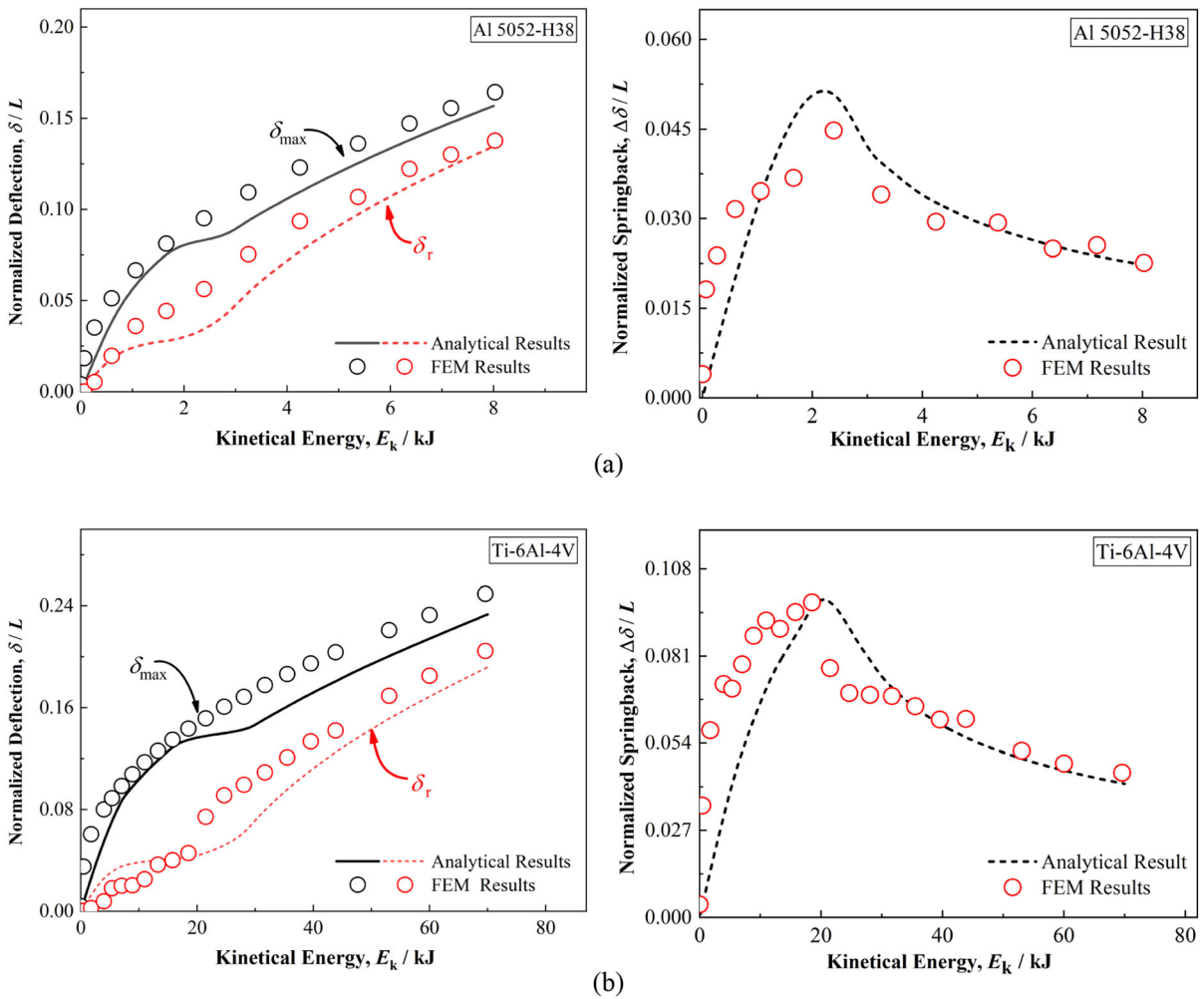
**Fig. 17** Comparison of normalized deflections (left figures) and springback (right figure) between analytical and numerical results for fully-clamped beam made of: **a** aluminum alloy (Al 5052-H38 (Khodaei et al. 2011)) and **b** titanium alloy [Ti-6Al-4 V (Yuan et al. 2021)]

**Fig. 18** Ratio of structural springback to residual deflection plotted as a function of ratio of kinetic energy to the threshold of stored elastic energy for fully-clamped beams made of selected metals. Hollow symbols represent FE simulation results and dashed lines denote envelope curves of the results
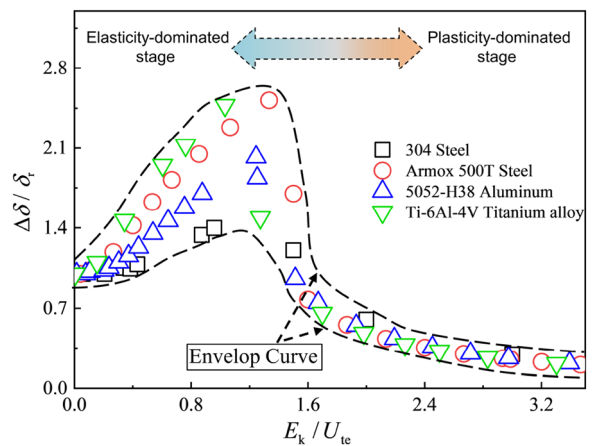
## 7 Conclusions

Based on experimental observations, a beam-hinge analytical model had been proposed to predict the dynamic deflection and springback of a fully-clamped metallic beam subjected to impulsive loading sufficiently large that a portion of the beam or the entire beam was plastically yielded. Finite element simulations were performed to validate the proposed model, with good agreement achieved. Physical mechanisms underlying springback were explored and key parameters affecting springback were investigated, including yield strength, strain hardening and strain rate. The following main conclusions were drawn:

1. The proposed analytical model was capable of describing adequately the three distinct stages of a dynamically loaded and fully-clamped metallic beam, although the validity of its predictions was restricted to metallic materials obeying approximately elastic-perfectly plasticity and to cases where either elastic or plastic deformation dominates the beam deflection but not both.

2. The springback of a fully-clamped metallic beam increases with increasing impulsive load within the elasticity-dominated stage, but decreases with increasing impulsive load in the plasticity-dominated stage.

3. The beam made of a metal having a higher yield strength possesses a higher loading capacity (i.e., a smaller peak deflection) and a greater capacity to store elastic strain energy, thus exhibits more significant springback.

4. Material strengthening due to strain hardening and strain rate effects also contributes to significantly enhanced loading capacity and storage of elastic deformation energy, leading to enlarged springback.

5. When subjected to impulsive loading, a protective structure should possess high impact resistance (low permanent deflection) as well as good predictability of impact resistance (low springback).

The present study offers new insights into the dynamic response of metallic structures subjected to impulsive loadings and are helpful for designing high-performance protective systems against intensive blast loadings.

## References

Chen, G., Chen, Z., Tao, J., et al.: Investigation and validation on plastic constitutive parameters of 45 steel (in Chinese). Explos. Shock Wave **25**(5), 451–456 (2005)

Da-Xin, E., He, H.H., Liu, X.Y., Ning, R.X.: Spring-back deformation in tube bending. Int. J. Miner. Metall. Mater. **16**(2), 177–183 (2009)

Gauch, H.L., Montomoli, F., Tagarielli, V.L.: The response of an elasto-plastic clamped beam to transverse pressure loading. Int. J. Impact Eng. **112**, 30–40 (2018)

Hawass, A., Mostafa, H., Elbeih, A.: Multi-layer protective armour for underwater shock wave mitigation. Def. Technol. **11**, 338–343 (2005)

Hosford, W.F., Caddell, R.M.: Metal forming: Mechanics and Metallurgy. Cambridge University Press, Cambridge (2007)

Iqbal, M.A., Senthil, K., Sharma, P., Gupta, N.K.: An investigation of the constitutive behavior of Armox 500T steel and armor piercing incendiary projectile material. Int. J. Impact Eng. **96**, 146–164 (2016)

Jones, N.: Structural Impact, 2nd edn. Cambridge University Press, Cambridge (2012)

Karthikeyan, K., Russell, B.P., Fleck, N.A., et al.: The soft impact response of composite laminate beams. Int. J. Impact Eng. **60**, 24–36 (2013)

Kyner, A., Deshpande, V., Wadley, H.N.G.: Momentum transfer during the impact of granular matter with inclined sliding surfaces. J. Mech. Phys. Solids **106**, 283–312 (2017a)

Kyner, A., Dharmasena, K., Williams, K., et al.: High intensity impulsive loading by explosively accelerated granular matter. Int. J. Impact Eng. **108**, 229–251 (2017b)

Khodaei, M., Mojtaba, H.-K., Safarabadi, M.: Numerical modeling of high velocity impact in sandwich panels with honeycomb core and composite skin including composite progressive damage model. J. Sandw. Struct. Mater. **22**, 2768 (2020)

Li, L., Zhang, Q.C., Zhao, Z.Y., et al.: A laboratory experimental technique for simulating combined blast and impact loading. Int. J. Impact Eng. **134**, 103382 (2019)

Li, M., Zong, Z., Du, M., et al.: Experimental investigation on the residual axial capacity of close-in blast damage CFDST columns. Thin. Wall. Struct. **165**, 107976 (2021)

Liu, T., Fleck, N.A., Wadley, H.N.G., et al.: The impact of sand slugs against beams and plates: coupled discrete particle/finite element simulations. J. Mech. Phys. Solids **61**, 1798–1821 (2013)

Marciniak, Z., Duncan, J.L., Hu, S.J.: Mechanics of Sheet Metal Forming, 2nd edn. Butterworth-Heinemann, Oxford (2002)

Nahshon, K., Pontin, M.G., Evans, A.G., et al.: Dynamic shear rupture of steel plates. J. Mech. Mater. Struct. **2**(10), 2049–2066 (2007)

Neuberger, A., Peles, S., Rittel, D.: Scaling the response of circular plates subjected to large and close-range spherical explosions. Part I: Air-blast loading. Int. J. Impact Eng. **34**, 859–873 (2007)

Neuberger, A., Peles, S., Rittel, D.: Springback of circular clamped armor steel plates subjected to spherical air-blast loading. Int. J. Impact Eng. **36**, 53–60 (2009)

Olovsson, L., Hanssen, A.G., Børvik, T., et al.: A particle-based approach to close-range blast loading. Eur. J. Mech. A **29**, 1–6 (2010)

Qiu, X., Deshpande, V.S., Fleck, N.A.: Impulsive loading of clamped monolithic and sandwich beams over a central patch. J. Mech. Phys. Solids **53**, 1015–1046 (2005)

Radford, D.D., Deshpande, V.S., Fleck, N.A.: The use of metal foam projectiles to simulate shock loading on a structure. Int. J. Impact Eng. **31**, 1152–1171 (2005)

Radford, D.D., Fleck, N.A., Deshpande, V.S.: The response of clamped sandwich beams subjected to shock loading. Int. J. Impact Eng. **32**, 968–987 (2006)

Rathbun, H.J., Radford, D.D., Xue, Z., et al.: Performance of metallic honeycomb-core sandwich beams under shock loading. Int. Solids Struct. **43**, 1746–1763 (2006)

Russell, B.P., Liu, T., Fleck, N.A., et al.: The soft impact of composite sandwich beams with a square-honeycomb core. Int. J. Impact Eng. **48**, 65–81 (2012)

Remennikov, A.M., Uy, B.: Explosive testing and modelling of square tubular steel columns for near-field detonations. J. Constr. Steel Res. **101**, 290–303 (2014)

Schleyer, G.K., Hsu, S.S.: A modelling scheme for predicting the response of elastic-plastic structures to pulse pressure loading. Int. J. Impact Eng. **24**, 759–777 (2000)

Schleyer, G.K., Hsu, S.S., White, M.D., et al.: Pulse pressure loading of clamped mild steel plates. Int. J. Impact Eng. **28**, 223–247 (2003)

Showichen, A.: Numerical Analysis of Vehicle Bottom Structures Subjected to Anti-tank Mine Explosions. Cranfield University, Cranfield (2008)

Shi, S., Zhu, L., Yu, T.X.: Elastic-plastic response of clamped square plates subjected to repeated quasi-static uniform pressure. Int. J. Appl. Mech. **10**(6), 1850067 (2018)

Tian, L.R., Chen, F.L., Zhu, L., et al.: Large deflection of square plates under pulse loading by combined saturation analysis and membrane factor methods. Inter. J. Impact Eng. **140**, 103546 (2020)

Wu, H., Peng, Y.L., Fang, Q.: Experimental and numerical study of ultra-high performance cementitious composites filled steel tube subjected to close-range explosion. Int. J. Impact Eng. **141**, 103569 (2020)

Xue, Z., Hutchinson, J.W.: A comparative study of impulse-resistant metal sandwich plates. Int. J. Impact Eng. **30**, 1283–1305 (2004)

Yuan, Z., Han, Y., Zang, S., et al.: Analysis of the mechanical properties of TiN/Ti multilayer coatings using indentation under a broad load range. Ceram Int. **47**, 10769–10808 (2021)

Yu, T.X., Qiu, X.M.: Introduction to Impact Dynamics. Tsinghua University Press, Beijing (2018)

Zakrisson, B., Wikman, B., Haggblad, H.-A.: Numerical simulation of blast loads and structural deformation from near-field explosions in air. Int. J. Impact Eng. **38**, 597–612 (2011)

Zhang, S.L., Liang, J., Guo, C.: A constitutive model for springback prediction in which the change of Young's modulus with plastic deformation is considered. Int. J. Mach. Tool Manu. **47**, 1791–1797 (2007)

Zheng, C., Kong, X., Wu, W., et al.: The elastic-plastic dynamic response of stiffened plates under confined blast load. Int. J. Impact Eng. **95**, 141–153 (2016)